

A Nearest-Neighbor Based Nonparametric Test for Viral Remodeling in Heterogeneous Single-Cell Proteomic Data

Trambak Banerjee¹, Bhaswar B. Bhattacharya² and Gourab Mukherjee³

¹University of Kansas, ²University of Pennsylvania and ³University of Southern California

Abstract

An important problem in contemporary immunology studies based on single-cell protein expression data is to determine whether cellular expressions are remodeled post infection by a pathogen. One natural approach for detecting such changes is to use nonparametric two-sample statistical tests. However, in single-cell studies, direct application of these tests is often inadequate, because single-cell level expression data from processed uninfected populations often contain attributes of several latent subpopulations with highly heterogeneous characteristics. As a result, viruses often infect these different subpopulations at different rates in which case the traditional nonparametric two-sample tests for checking similarity in distributions are no longer conservative. In this paper, we propose a new nonparametric method for *Testing Remodeling Under Heterogeneity* (TRUH) that can accurately detect changes in the infected samples compared to possibly heterogeneous uninfected samples. Our testing framework is based on composite nulls and is designed to allow the null model to encompass the possibility that the infected samples, though unaltered by the virus, might be dominantly arising from under-represented subpopulations in the baseline data. The TRUH statistic, which uses nearest neighbor projections of the infected samples into the baseline uninfected population, is calibrated using a novel bootstrap algorithm. We demonstrate the non-asymptotic performance of the test via simulation experiments, and also derive the large sample limit of the test statistic, which provides theoretical support towards consistent asymptotic calibration of the test. We use the TRUH statistic for studying remodeling in tonsillar T cells under different types of HIV infection and find that unlike traditional tests which do not have any heterogeneity correction, TRUH based statistical inference conforms to the biologically validated immunological theories on HIV infection.

Keywords: single-cell virology, immunology, two-sample tests, viral remodeling, homogeneous Poisson process, nearest neighbors, HIV infection, mass cytometry.

³The research here was partially supported by NSF DMS-1811866.

³Corresponding author: gmukherj@marshall.usc.edu

1 Introduction

In many contemporary scientific methodologies, it is extremely difficult, even in well-regulated laboratory experiments, to simultaneously control the multitude of factors that give rise to heterogeneity in the population (Chapter 3 of [Holmes and Huber \(2018\)](#)). Nevertheless, these experiments are very powerful, and are often our only recourse to study several interesting biological phenomena. For example, in single-cell proteomic and genomic studies ([Jia et al. \(2017\)](#), [Jiang et al. \(2018\)](#), [Shi and Huang \(2017\)](#), [Wang et al. \(2018\)](#)), it is now well understood that there is high heterogeneity in cellular responses from controlled cell population. Statistical tests are often used on these datasets to determine differences between the case and control samples. The presence of heterogeneity greatly complicates statistical inference, and direct application of existing two-sample testing methods, without modulating for the latent heterogeneity in the samples, may lead to erroneous statistical decisions and scientific consequences. The problem of testing similarity in the distributions of two samples under heterogeneity arises in a host of modern immunology research set-ups where heterogeneous protein expression datasets collected at single-cell resolution are analyzed to detect viral perturbation. To provide a rigorous statistical hypothesis testing framework for these immunology studies, we consider a composite null hypothesis that allows mixture expression distributions in cases and controls with the mixture having same components but potentially different mixing proportions; the alternative hypothesis contains scenarios where at least one of the mixture components is actually different between the cases and the controls. We develop a new nonparametric testing procedure based on nearest-neighbor distances, that can accurately detect if there are differences between the case and control samples in the presence of unknown heterogeneity in the data-generation process. We next provide the background of the problem through an immunology study on human immunodeficiency virus (HIV) infection in tonsillar cells.

1.1 Phenotypic Profiling of T Cells Under HIV Infection

In single-cell immunology, phenotypic profiling of immune cells under the influence of a target virus, such as the HIV ([Cavrois et al., 2017](#)), the varicella zoster virus (VZV) ([Sen et al., 2014](#)), or the rotavirus (RV) ([Sen et al., 2012](#)), is a critical research endeavor. It enhances understanding of which subsets of cells are most or least susceptible to infection, leading to new insights regarding the magnitude of viral persistence, which is crucial in the development of life saving drugs ([Sen et al., 2015](#)). Mass cytometry based techniques ([Bendall et al., 2011](#), [Giesen et al., 2014](#)) are popularly used for generating proteomic datasets for such phenotypic analysis. These techniques can simultaneously measure around fifty protein expressions on individual cells. In this paper we provide a rigorous statistical analysis for testing if

there are any HIV induced changes in the proteomic expressions of tonsillar T cells, which are a type of lymphocyte that plays a central role in the immune response, based on the dataset generated in (Cavrois et al., 2017).

Figure 1 presents a schematic representation of the experimental set-up used for generating single-cell level proteomic expression data of HIV infected T cells using Cytometry by Time Of Flight (CyTOF) technique. Tonsillar T cells from 4 healthy donors were infected with two variants of a HIV viral strain: *Nef rich* HIV and *Nef deficient* HIV. *Nef* (Negative Regulatory Factor) is a protein encoded by HIV which enhances virus replication in the host cell by protecting infected cells from immune surveillance. We study the differential impact of these two variants on the immune cells. The healthy cells were cultured and processed into three batches for each donor. For each patient, one among the three batches were randomly selected and phenotyped to generate the expression data of the uninfected population, while the other two batches were contaminated with the *Nef rich* HIV and the *Nef deficient* HIV, respectively, and phenotyped after 4 days of infection. All the batches were phenotyped using multi-parameter CyTOF panel which contained 35 surface markers and 3 viral markers. These are special proteins attached to the cell membrane. After leaving out dead cells from each run of the CyTOF experiment we had 38 protein expressions for approximately 25,000 uninfected cells. Virus infected cell in the contaminated population were marked based on the expression of the viral markers and it was found that the number of virally infected cells in the batch subjected to HIV infection was around 250. These cells constitute the infected cell population.

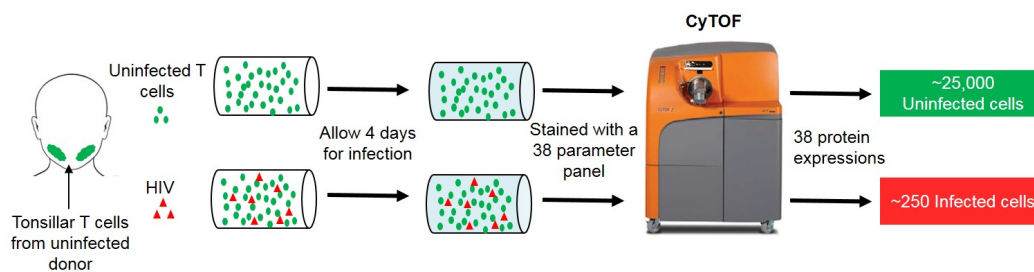


Figure 1: Schematic representation of the experimental design associated with the phenotypic analysis of HIV infected CD4+ T cells using mass cytometry. Tonsillar T cells from a healthy donor (represented by green circles) are infected with the *Nef rich* or the *Nef deficient* HIV virus (represented by red triangles). These cells were then phenotyped in a 38 parameter panel after allowing 4 days for infection. The resulting data has 38 protein expressions for approximately 25,000 uninfected cells and the number of virally infected cells was around 250.

1.2 Viral Remodeling

If the virus changes the expression of any of the surface markers, which are proteins attached to the cell membrane, then the cell is said to have undergone viral remodeling of its phenotypic characteristics (Sen et al., 2014). A virally remodelled cell will have aberrant inter-cellular activities, therefore, detecting

the presence of remodeling is a fundamental step towards understanding the mechanism of pathogenesis and disease progression. Detecting remodeling translates to testing if there is enough evidence in the data to reject the null hypothesis that the joint distribution of all the surface proteins is same between the uninfected and virus infected sample. A natural approach for this problem is to invoke nonparametric two-sample testing methods to see if there is enough evidence to support the alternative hypothesis that the virus has changed the distribution of least one of the subpopulations. However, for single-cell level expression data, the hypothesis test described above is particularly difficult because of the following two reasons: (a) the presence of *heterogeneity* in the uninfected population, and (b) due to the phenomenon of *preferential infection*. Single-cell resolution expression data from processed uninfected population often contains attributes from several latent subpopulations with highly heterogeneous characteristics. This subpopulation level heterogeneity in the uninfected (also referred to as the control or baseline) samples can arise from varied attributes that cannot be controlled in experiments, such as differences in the cell effector functions, trafficking and longevity (Cavrois et al., 2017). Viruses often infect these different subpopulations at different rates. If a virus infects different subpopulation at different rates, but does not alter the marker expressions for any of the subpopulations, still the distribution of the overall viral sample will be different from the uninfected samples. In these situations, the difference in distribution between the infected and the uninfected samples is not due to *viral remodeling* but due to *preferential infection* (for a detailed biological explanation see Figures 2A and 2B of (Cavrois et al., 2017)) of the uninfected subpopulations by the virus.

Figure 2 presents two scenarios that may arise when the cloud of infected and uninfected cells are analyzed with respect to a single marker *A*. In this toy example, Panel 1 in Figure 2 shows that the uninfected T cells arise from three subpopulations with varying expression levels for marker *A* which may reflect their inherent heterogeneity with respect to cell longevity. The scenario of *preferential infection* is depicted in Panel 2 where the HIV preferentially infects the T cell subpopulation that has a lower expression level for marker *A* amongst the uninfected cells. Moreover, the virus does not alter the expression levels of these infected cells when compared to Panel 1. In Panel 3, which represents *HIV remodeling*, the virus targets those uninfected cells that have low to medium expression for marker *A* amongst the uninfected cells and alters their original expression levels upon infection. The distinct pink and yellowish shade of the infected cells in panel 3 depicts their phenotypic change associated with infection. Here, we have described the phenomenon of viral remodeling only for the HIV. However, remodeling analysis is widely conducted across virology for understanding mechanism of other pathogens also. For correct scientific understanding of the viral mechanism, it is extremely important to accurately distinguish the instances of viral remodeling from mere preferential infection. However, popular single-cell based segmentation and

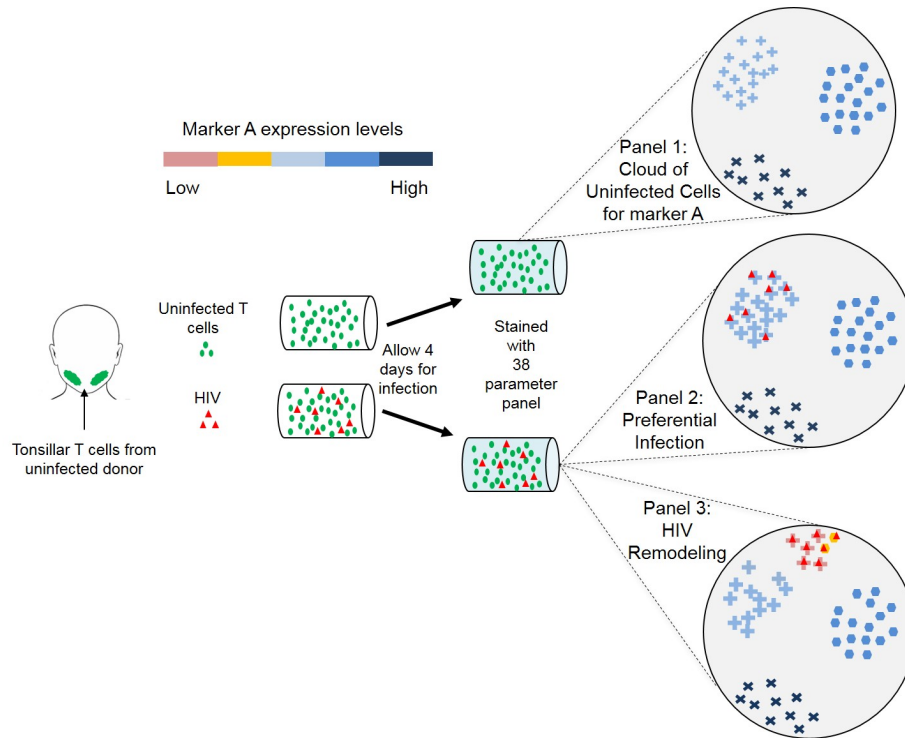


Figure 2: Schematic representation of HIV remodeling of T cells with respect to a single marker *A*. Panel 1 shows that the uninfected T cells arise from three subpopulations with varying expression levels for marker *A*. Panel 2 depicts *preferential infection* where the HIV preferentially infects the T cell subpopulation that has a lower expression level for marker *A* amongst the uninfected cells and the infection does not alter the expression levels of the T cells when compared to Panel 1. Panel 3 represents *HIV remodeling* where the HIV targets those uninfected cells that have low to medium expression for marker *A* amongst the uninfected cells and alters their original expression levels upon infection, which is represented by the distinct pink and yellowish shade of the infected cells.

classification algorithms (Amir et al., 2013, Bruggner et al., 2014, Linderman et al., 2012, Qiu, 2012) lack a rigorous statistical hypothesis testing framework for conducting two-sample inference and can greatly suffer in testing problems, particularly if there is high imbalance in the sizes of the uninfected (control) and infected (case) samples, which is often the situation in virology.

1.3 Testing Procedures in Existing Literature and Statistical Challenges

The statistical framework for testing remodeling falls under the realm of nonparametric two-sample testing. For univariate data, nonparametric two-sample tests like the Kolmogorov-Smirnov test, the Wilcoxon rank-sum test, and the Wald-Wolfowitz runs test are extremely popular and find a place in every practitioner’s toolkit. Multidimensional versions of these widely used tests date back to the randomization tests of Chung and Fraser (1958) and to the generalized Kolmogorov-Smirnov test of Bickel (1969). Friedman and Rafsky (Friedman and Rafsky, 1979) proposed the first computationally efficient nonparametric two-sample test, which applies to high-dimensional data. The Friedman-Rafsky edgcount test, which can be viewed as a generalization of the univariate runs test, computes the Euclidean minimal spanning

tree (MST)¹ of the pooled sample, and rejects the null if the number of edges with endpoints in different samples is small. Many variants of the edgcount test, based on nearest-neighbor distances and geometric graphs have been proposed over the years [Hall and Tajvidi \(2002\)](#), [Henze \(1984\)](#), [Rosenbaum \(2005\)](#), [Schilling \(1986\)](#), [Weiss \(1960\)](#). Recently, [Chen and Friedman \(2017\)](#) suggested novel modifications of the edge-count test for high-dimensional and object data, and [Chen et al. \(2018\)](#) proposed new and powerful tests to deal with the issue of sample size imbalance. Asymptotic properties of two-sample tests based on geometric graphs can be studied in the general framework described in [Bhattacharya \(2019\)](#). Other popular two-sample tests include the test of [Baringhaus and Franz \(2004\)](#), the energy distance test of [Aslan and Zech \(2005\)](#), and the kernel based test using maximum mean discrepancy of [Gretton et al. \(2007\)](#). More recently, [Chen et al. \(2013\)](#) address the problem of sample size imbalances in the two-sample problem by constructing an ensemble subsampling scheme for the nearest-neighbor tests [Henze \(1984\)](#), [Schilling \(1986\)](#). Very recently, [Deb and Sen \(2019\)](#) and [Ghosal and Sen \(2019\)](#) proposed distribution-free two-sample tests based on the concept of multivariate ranks, defined using optimal transport. Methods based on nearest neighbor distances have been also used extensively in other non-parametric statistical problems, such as density estimation [Mack \(1983\)](#), [Mack and Rosenblatt \(1979\)](#), nonparametric clustering [Heckel and Bölskei \(2015\)](#), classification [Cannings et al. \(2019\)](#), [Cover and Hart \(1967\)](#), [Gadat et al. \(2016\)](#), [Samworth \(2012\)](#), entropy and other functional estimation [Berrett and Samworth \(2019a\)](#), [Berrett et al. \(2019\)](#), [Kozachenko and Leonenko \(1987\)](#) and testing problems, such as testing for normality [Vasicek \(1976\)](#), testing for uniformity [Cressie \(1976\)](#), and independence testing [Berrett and Samworth \(2019b\)](#), [Goria et al. \(2005\)](#).

One of the main challenges for devising a statistically correct test to detect viral remodeling from preferential infection is that the virus may infect different subpopulations at different rates. In [Section 2](#), we show that even in very large sample sizes direct application of existing nonparametric two-sample tests can lead to erroneous inference. We expound this phenomenon by exhibiting explicit scenarios of preferential infection and remodeling where traditional tests fail in a simple setting of $d = 2$ markers. In [Figure 3](#), the green triangles correspond to a sample of uninfected (UI) cells that arise from three different subpopulations while the red dots reflect the infected (VI) cells. The leftmost panel presents a setting where the virus has infected all the three cellular subpopulations and the overlap of the UI and VI cells indicate no remodeling. The middle panel presents a scenario where the cells have undergone remodeling under the influence of the virus as is evident through a shift in the location of the VI cells. The rightmost panel reflect no remodeling but preferential infection. The different g -tests ([Chen et al., 2018](#), [Chen and Friedman, 2017](#), [Friedman and Rafsky, 1979](#)), the cross-match test ([Rosenbaum,](#)

¹Given a finite set $S \subset \mathbb{R}^d$, the *minimum spanning tree* (MST) of S is a connected graph with vertex-set S and no cycles, which has the minimum weight, where the weight of a graph is the sum of the distances of its edges.

2005), and the energy test (Aslan and Zech, 2005) reject the null hypothesis of no remodeling in all the three cases, in each of the 100 simulation replications (see Table 3 in Section 3.1). This is not surprising, because these tests are designed to test the simple null hypothesis of equality of the two distributions.

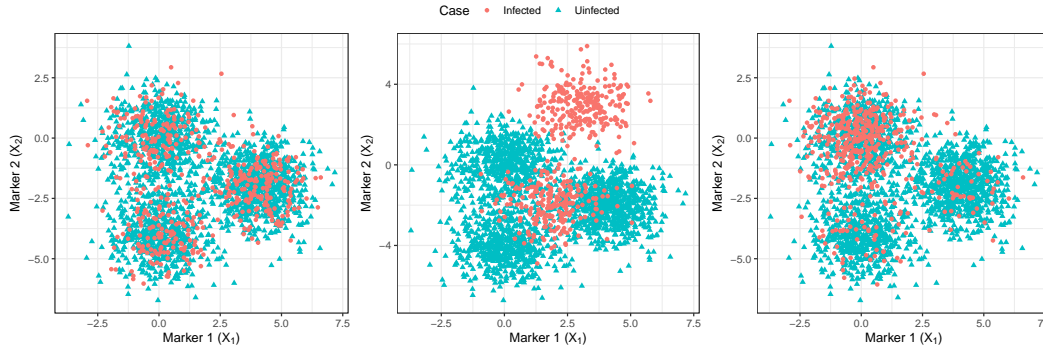


Figure 3: Schematic representation of viral remodeling of infected cells versus preferential viral infection with respect to $d = 2$ markers, X_1 and X_2 . From left to right, we have (a) no remodeling, (b) remodeling, and (c) no remodeling, but preferential infection. Uninfected cells are in green whereas virus infected cells are in red.

Due to the presence of subpopulation level heterogeneity the problem of testing for remodeling warrants testing a composite null hypothesis. To this end, note that under preferential infection, the two samples arise from the mixture distribution with identical component distributions but with different mixing weights. This is the case for the right most subplot in Figure 3. In this paper, we formulate the problem of testing for preferential infection versus remodeling as a composite two-sample hypothesis with mixture distributions, and develop a new nearest-neighbor based test that can consistently and efficiently detect the differences between the two samples.

1.4 The TRUH Testing Framework: Novel attributes and Our Contributions

In this article, we propose a novel procedure for *Testing Remodeling Under Heterogeneity* (TRUH), that effectively incorporates the underlying heterogeneity and imbalance in the samples, and provides a conservative test for the composite null hypothesis that the two samples arise from the same mixture distribution but may differ with respect to the mixing weights. We summarize its key attributes below:

- The TRUH statistic is based on a nearest neighbor approach (Cover and Hart, 1967, Devroye et al., 2013) that relies on first identifying for every infected cell a predictive precursor cell which is the phenotypically closest cell in the uninfected population. It then measures the relative dissimilarities between the infected cells and their predictive precursors and the predictive precursors to their most phenotypically similar uninfected cells. A large relative dissimilarity between the infected cells and their predictive precursors indicates surface protein regulation or remodeling by the virus, while a small relative dissimilarity provides evidence for preferential infection or no remodeling.

- We describe an efficient bootstrap based approach for calibrating the `TRUH` test statistic, and evaluate its performance in finite-sample simulations. We then use this method to test for viral remodeling in tonsillar T cells under different types of HIV infection, corroborating the efficacy of our proposed procedure.
- We provide an extensive theoretical understanding of the large sample characteristics of our proposed test statistics. We establish the L_2 -limit of our proposed statistic using asymptotic properties of functionals of random geometric graphs [Penrose and Yukich \(2003\)](#). The limit can be expressed in terms of the densities of the uninfected and infected populations and dimension dependent constants obtained from nearest-neighbor distances defined on a homogeneous Poisson process. Using these properties, we can select a cut-off for the `TRUH` statistic that is asymptotically consistent against biologically-relevant location alternatives. Traditional nonparametric tests enjoy these consistency properties in homogeneous populations but not under heterogeneity. We show that using a nearest neighbor based approach this inefficiency of existing nonparametric tests in heterogeneous data can be mitigated.

The rest of the paper is organized as follows: In [Section 2](#), we formulate the problem of testing for remodeling in single-cell virology as a heterogeneous two-sample problem, describe the `TRUH` framework, and show how it can be calibrated using the bootstrap. Numerical experiments demonstrating the non-asymptotic performance of our testing procedure are given in [Section 3](#). In [Section 4](#) we use `TRUH` for studying remodeling in tonsillar T cells under different types of HIV infection. The asymptotic properties of the test statistic are discussed in [Section 5](#). We conclude the paper in [Section 6](#) with a discussion. The technical details and proofs of the theoretical results are given in the supplementary materials.

2 Statistical Framework and the Proposed `TRUH` Statistic

In this section we formulate the problem of testing for remodeling in single-cell virology as a heterogeneous two-sample problem ([Section 2.1](#)), introduce the `TRUH` statistic ([Section 2.2](#)), and discuss how to calibrate it using the bootstrap ([Section 2.3](#)).

2.1 The Heterogeneous Two-Sample Problem

In our virology example, the baseline constitutes the m uninfected cells. For each cell, $i \in \{1, \dots, m\}$, we denote by U_i a d -dimensional vector of cellular characteristics typically measuring expressions corresponding to different genes or proteins. Denote the uninfected/baseline population by $U_m = \{U_1, \dots, U_m\}$.

Let F_0 be the cumulative distribution function (cdf) of the baseline population with the heterogeneity in the population being reflected by K different subgroups each having unimodal distributions with distinct modes and cdfs F_1, \dots, F_K , and mixing proportions w_1, \dots, w_K , such that

$$F_0 = \sum_{a=1}^K w_a F_a, \quad \text{where } w_a \in (0, 1) \text{ and } \sum_{a=1}^K w_a = 1. \quad (1)$$

Note that, the number of components K , the mixing distributions F_1, \dots, F_K , and the mixing weights w_1, \dots, w_K are fixed (non-random) attributes, which are unknown. Also, as F_1, \dots, F_K are cdfs from unimodal distributions with distinct modes, F_0 is well-defined with a unique specification. In addition to the uninfected population, we observe n i.i.d. infected observations $V_n = \{V_1, \dots, V_n\}$ from a distribution function G in \mathbb{R}^d . Note that, the infected and uninfected samples U_m and V_n are collected from separate experiments and are independent of each other.

Simple versus Composite Null In single-cell virology when an uninfected population is exposed to a pathogen, the virus may infect the different subpopulations at different rates. Therefore, even if the virus does not cause any change in the cellular characteristics, the virus infected sample might have different representations of the uninfected subpopulations than the uninfected mixing proportions $\{w_1, \dots, w_K\}$. As such, it is quite possible that a few of uninfected subpopulations are completely absent in the viral population, which biologically implies that the virus preferentially targets few cellular subpopulations. Thus, if the virus does not induce any change in the cellular characteristics, then the distribution of the infected population G lies in a class of distributions $\mathcal{F}(F_0)$ that contains any convex combination of $\{F_1, \dots, F_K\}$ including the boundaries, that is,

$$\mathcal{F}(F_0) = \left\{ Q = \sum_{a=1}^K \lambda_a F_a : \lambda_1, \lambda_2, \dots, \lambda_K \in [0, 1] \text{ and } \sum_{a=1}^K \lambda_a = 1 \right\}. \quad (2)$$

Note that the uninfected cdf F_0 is a particular member of the class $\mathcal{F}(F_0)$. If the virus induces changes in the cellular characteristics, then the viral population distribution would contain at least one nontrivial subpopulation with distribution substantially different from $\{F_1, F_2, \dots, F_K\}$ or their linear combinations. Thus, the test for viral remodeling tantamounts to testing the following composite null hypothesis:

$$H_0 : G \in \mathcal{F}(F_0) \quad \text{versus} \quad H_A : G \notin \mathcal{F}(F_0). \quad (3)$$

If the null hypothesis is accepted, we say the virus exhibits *preferential infection*, otherwise we say the virus exhibits *remodeling* (see Figure 6 below), and the hypothesis testing problem (3) will be referred

to as the problem of *testing remodeling under heterogeneity* (TRUH). Later on, to facilitate proofs of the theoretical properties of our proposed method, we will assume that the baseline cdfs F_1, \dots, F_K have unimodal densities f_1, \dots, f_K (with respect to Lebesgue measure). In this case, the baseline uninfected population will have density $f_0 = \sum_{a=1}^K w_a f_a$, and the set of distributions in (2) can be represented in terms of the densities f_1, \dots, f_K , and will be denoted by $\mathcal{F}(f_0)$.

Inefficiency of Existing Tests Traditional nonparametric graph-based two-sample tests, such as the edgecount (EC) test of [Friedman and Rafsky \(1979\)](#) or the crossmatch (CM) test of [Rosenbaum \(2005\)](#), are tailored for the null hypothesis $H_0 : F_0 = G$, that is, testing whether the distributions of the uninfected samples U_m and the infected samples V_n are the same. However, not surprisingly, direct application of these tests to the composite hypothesis testing problem described in (3) above gives non-conservative procedures. To see this, consider the EC test. Recall that the EC test is based on the statistic $\mathcal{R}(U_m, V_n)$ which counts the number of edges in the minimal spanning tree (MST) of the pooled sample $\{U_1, \dots, U_m, V_1, \dots, V_n\}$ that connect points from different samples. Then, the EC test rejects the null hypothesis of $F_0 = G$ for small values of $\mathcal{R}(U_m, V_n)$. The cut-off for $\mathcal{R}(U_m, V_n)$ can be chosen based on the asymptotic distribution $\mathcal{R}(U_m, V_n)$ under $F_0 = G$, which was derived by [Henze and Penrose \(1999\)](#) in the usual limiting regime where $m, n \rightarrow \infty$ and $n/m \rightarrow \rho \in (0, \infty)$. In particular, it follows from Theorem 1 of [Henze and Penrose \(1999\)](#) that

$$\lim_{m, n \rightarrow \infty} \mathbb{P}_{F_0=G}(\mathcal{R}(U_m, V_n) < C_{m,n}(\alpha)) = \alpha, \quad (4)$$

with $C_{m,n}(\alpha) = \frac{2mn}{m+n} - z_{1-\alpha} \sigma_d \sqrt{m+n}$, where $z_{1-\alpha}$ is the α -th quantile of the standard normal distribution, $\sigma_d^2 = \rho(4\rho + (1-\rho)^2 \delta_d)/(1+\rho)^4$, and δ_d is a constant depending only on dimension d . More precisely, δ_d is the variance of the degree of the origin $\mathbf{0} \in \mathbb{R}^d$ in the minimal spanning tree built on a homogeneous Poisson process of rate 1 in \mathbb{R}^d with the origin added to it. Note that (4) shows that the test with rejection region $\{\mathcal{R}(U_m, V_n) < C_{m,n}(\alpha)\}$ is asymptotically level α for the null hypothesis of $F_0 = G$.

The following proposition shows that direct application of the EC test as described above, will not be conservative for testing the hypothesis (3) of viral remodeling. In fact, for cases of preferential infection but no remodeling the EC test will produce undesired false discoveries.

Proposition 1. *Fix $\alpha \in (0, 1/2)$. Then for F_0 as in (1) and for any $G \in \mathcal{F}(F_0) \setminus \{F_0\}$ in the usual limiting regime,*

$$\lim_{m, n \rightarrow \infty} \mathbb{P}(\mathcal{R}(U_m, V_n) < C_{m,n}(\alpha)) = 1,$$

with $\mathbf{U}_m = \{U_1, \dots, U_m\}$ i.i.d. from f_0 and $\mathbf{V}_n = \{V_1, \dots, V_m\}$ i.i.d. from g , where f_0 and g are the densities (with respect to the Lebesgue measure) of F_0 and G , respectively.

The proof of the above result is given in the supplementary materials (Section A). This shows that for any level α , the EC test will be inconsistent as it would reject with certainty all cases of preferential infection but no remodeling. This phenomenon is demonstrated in Figure 4 through a simple univariate simulation experiment. Here, we consider $m = 1000$, $n = 50$, and $d = 1$. The true distribution of the

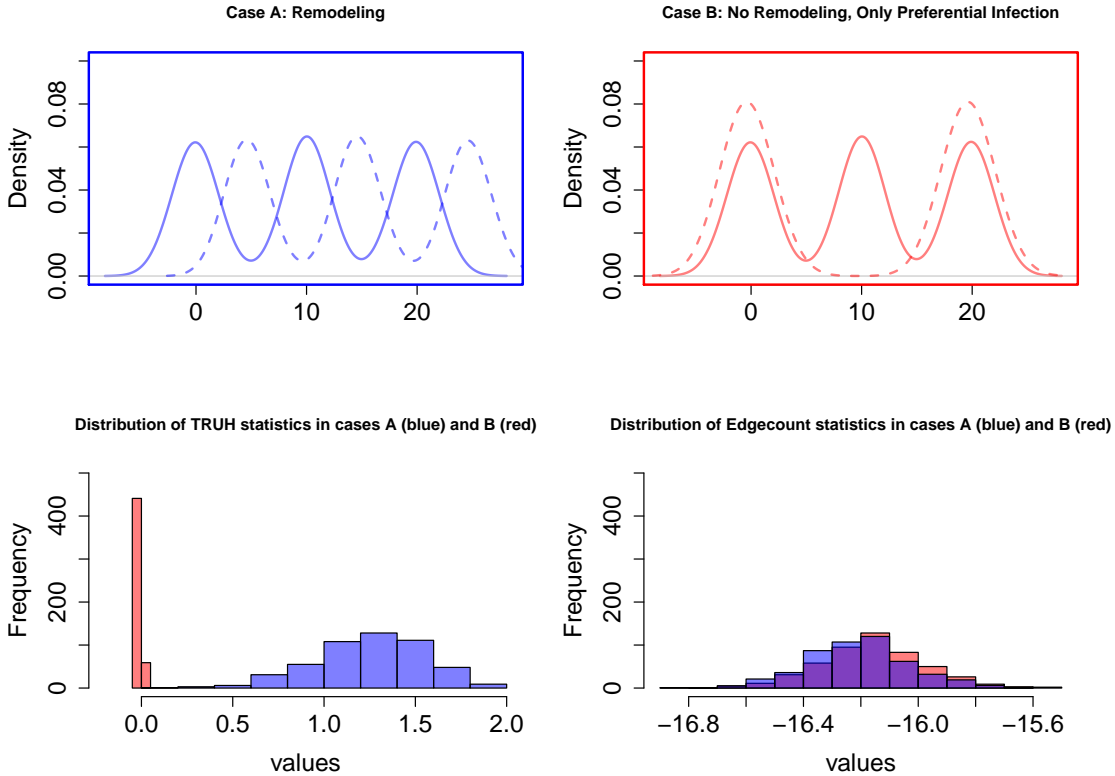


Figure 4: Simulation example showing the performance of edgccount test statistic versus the TRUH statistic. In the top row, we describe the density of the true uninfected F_0 (in continuous line) and the density of the infected G (in dotted line) for the two cases. In both cases, F_0 and G are mixtures of normal distributions. In the first case, all the three equiprobable subpopulations in F_0 have undergone a discernible location change in G . In case B, F_0 again has three equiprobable subgroups while G has two of those three subgroups. Thus, while case A signifies viral remodeling, there is no remodeling but only preferential infection in Case B. In the bottom row, we have the histogram of the values of the TRUH statistic in the left (defined below in (7)) and the edgccount statistic in the right, respectively, under the two cases.

uninfected and infected subpopulations are gaussian mixtures. We consider two cases:

- *Case A:* Here, F_0 and G are equal-weighted mixtures of 3 Gaussians, with each subpopulation in G having a different mean from those in F_0 , that is, $F_0(u) = \frac{1}{3} \sum_{a=0}^2 \Phi(u - 4a)$ and $G(u) =$

$\frac{1}{3} \sum_{a=0}^2 \Phi(u - 4a - 2)$.² This is a clear case of viral remodeling.

- *Case B*: Here, $F_0 = \frac{1}{3} \sum_{a=0}^2 \Phi(u - 10a)$ and $G = \frac{1}{2} \sum_{a=0}^1 \Phi(u - 20a)$. In this case, there is preferential infection, but no remodeling, that is, $G \in \mathcal{F}(F_0)$ with the middle population in F_0 being resistant to viral infection.

Any test for the hypothesis (3) should ideally reject Case A and fail to reject Case B. However, Figure 4 shows that the histogram of EC test statistic values across 500 replications under cases A and B have a significant overlap. Table 1 shows the rejection rate (proportion of false discoveries) in Case B and power (proportion of true discoveries) in case A as the level of the test is varied. From the table it is evident that there does not exist any choice of a critical value such that the rejection rate of the EC test in Case B is commendable as it rejects all cases of preferential infection presented under Case B. On the other hand, our proposed test statistic (TRUH), described in the following section, entertains possibilities where both the rejection rate and the power attain the desired limit.

Table 1: The rejection rate and the power of the edgcount and TRUH test statistics across 500 repetitions of the simulation setting of Figure 4.

	Level	0.01	0.05	0.10	0.20
Power in Case A	edgcount	1.000	1.000	1.000	1.000
	TRUH	1.000	1.000	1.000	1.000
Rejection rate in Case B	edgcount	1.000	1.000	1.000	1.000
	TRUH	0.000	0.000	0.000	0.038

2.2 Proposed Test Statistic: TRUH

In this section we describe a nearest-neighbor based statistic for testing the hypothesis of remodeling. To this end, recall that $\mathbf{U}_m = \{U_1, \dots, U_m\}$ is the uninfected sample and $\mathbf{V}_n = \{V_1, \dots, V_n\}$ is the infected sample. Now, for each infected sample $V_i \in \mathbf{V}_n$, let

$$D_i = \min_{1 \leq j \leq m} \|V_i - U_j\|, \quad (5)$$

the Euclidean distance of V_i to its nearest point in the uninfected sample \mathbf{U}_m . The point in \mathbf{U}_m which attains this minimum will be denoted by $N(V_i, \mathbf{U}_m)$ ³ and constitutes a key point in \mathbb{R}^d for measuring the relative phenotypic difference between the infected cells and their closest uninfected counterparts. In Figure 5 we show the boxplots of the coordinates of $N_{\mathbf{V}_n, \mathbf{U}_m} = \{N(V_i, \mathbf{U}_m) : 1 \leq i \leq n\}$ in green, for

²Throughout, $\Phi(\cdot)$ and $\phi(\cdot)$ will denote the standard normal distribution function and density function, respectively.

³Given a finite set S and any point $x \in \mathbb{R}^d$, denote by $N(x, S) = \arg \min_{y \in S} \|x - y\|$, that is the nearest neighbor of x in the set S . If there is a tie, that is, $N(x, S)$ has multiple elements, then we choose a random element from them and set that to $N(x, S)$. However, if the underlying distribution of the data has a continuous density, then there are no ties with probability 1.

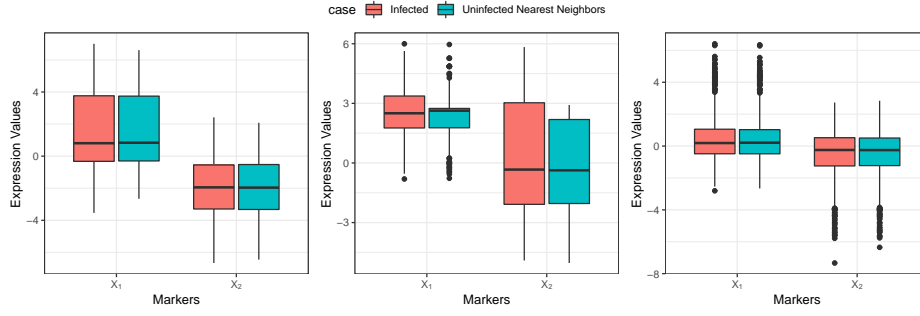


Figure 5: Boxplots of the coordinates of $N_{\mathbf{V}_n, \mathbf{U}_m} = \{N(V_i, \mathbf{U}_m) : 1 \leq i \leq n\}$ in green, adjacent to the boxplots of the coordinates of the corresponding infected cells \mathbf{V}_n in red, for each of the scenarios discussed under Figure 3. Recall that from left to right, we have (a) no remodeling, (b) remodeling, and (c) no remodeling, but preferential infection.

each of the scenarios discussed under Figure 3. Recall from Figure 3 that we have from left to right, (a) no remodeling, (b) remodeling, and (c) no remodeling, but preferential infection. We note that for scenarios (a) and (c), the distributions of $N_{\mathbf{V}_n, \mathbf{U}_m}$ and \mathbf{V}_n appear to overlap. However, in the case of remodeling (scenario (b) in the center plot), there is a clear difference between the two distributions for both the markers. The TRUH statistic captures this phenomenon and deals with the presence of heterogeneous groups (which can make the density within the uninfected sample \mathbf{U}_m to vary greatly), by comparing D_i with a feature of the local density of \mathbf{U}_m at $N(V_i, \mathbf{U}_m)$. For that purpose, define, for each infected observation,

$$C_i = \min_{1 \leq j \leq m: U_j \neq N(V_i, \mathbf{U}_m)} \|N(V_i, \mathbf{U}_m) - U_j\|, \quad (6)$$

which is the distance of $N(V_i, \mathbf{U}_m)$ to its nearest neighbor in \mathbf{U}_m . Our proposed test statistic for testing (3), hereafter referred to as the TRUH statistic, is

$$T_{m,n} = \frac{1}{n^{1-\frac{1}{d}}} \left| \sum_{i=1}^n (D_i - C_i) \right| = n^{\frac{1}{d}} |\bar{D}_{m,n} - \bar{C}_{m,n}|, \quad (7)$$

where $\bar{D}_{m,n} = \frac{1}{n} \sum_{i=1}^n D_i$ and $\bar{C}_{m,n} = \frac{1}{n} \sum_{i=1}^n C_i$. Note that the TRUH statistic above is an aggregated measure of how far apart each viral cell is from the uninfected sample compared to the local distance between uninfected sample points in its vicinity. Consider, for example, panel A in Figure 6 that represents a schematic for remodeling, while panel B depicts preferential infection. Here, the three infected cells (in red) in Panel A are phenotypically different than their uninfected counterparts and thus the average gap $|\bar{D}_{m,n} - \bar{C}_{m,n}|$ in Panel A, averaged over the three infected cells, is relatively larger than what is observed under preferential infection in Panel B. Therefore, we develop a test to reject the null hypothesis of no

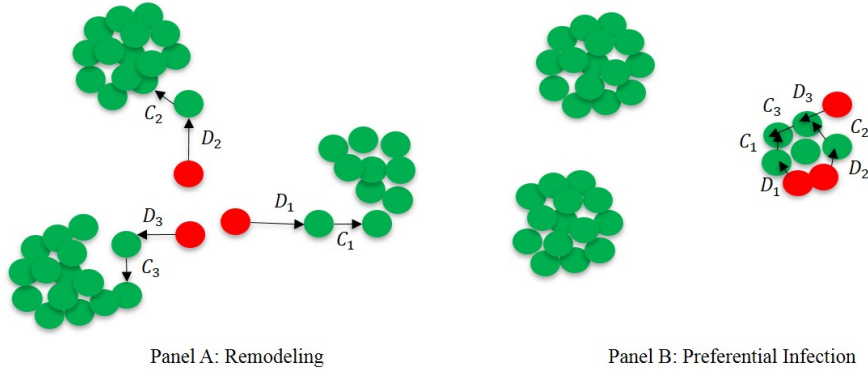


Figure 6: Panel A represents the scenario of remodeling while Panel B exhibits Preferential Infection. Uninfected cells are in green while infected cells are in red. The gaps are larger in case of remodeling as infected cells are phenotypically different than their uninfected counterparts.

remodeling for large values of $T_{m,n}$. The cut-off for $T_{m,n}$ can be chosen based on a bootstrap calibration (Section 2.3) or using the asymptotic limit of $T_{m,n}$ (Section 5). Note that, since the nearest neighbor of a point, in a cloud of n random points in \mathbb{R}^d , typically lies within a ball of radius $n^{-\frac{1}{d}}$ centered at that point, the TRUH statistic is scaled by $n^{1-\frac{1}{d}}$, which makes $T_{m,n}$ bounded in probability.

One of the interesting properties of the quantity $T_{m,n}$ is that it only involves enumeration of distance based features for the viral sample, unlike classical graph-based two-sample tests (Friedman and Rafsky, 1979, Rosenbaum, 2005) which are built using the inter-point distances of the pooled sample. As a consequence, the TRUH test statistic is not symmetric in its usage of the uninfected and infected samples, even when the sample sizes are equal and the two samples were actually generated from the same population distribution. This asymmetric sample usage of TRUH helps in tackling possibly different heterogeneity levels in the two samples. Finally, note that even though the quantities D_i and C_i are defined above using the Euclidean distance, they can be easily generalized to any arbitrary distance function, and the statistic $T_{m,n}$ can potentially be used in non-Euclidean data spaces, such as graph data or functional data, as well.

2.3 Bootstrap Based Calibration for TRUH

In this section, we present a bootstrap based procedure to determine the cut-off $t_{m,n,\alpha}$ for a level α test using $T_{m,n}$. To this end, recall that $\mathcal{F}(F_0)$ contains any convex combination of the baseline distribution functions $\{F_1, \dots, F_K\}$. Therefore, the proposed bootstrap procedure relies on the following two steps: (i) random sampling of the mixing proportions a large number of times, and (ii) for each such sampled mixing proportion, surrogate samples from $\mathcal{F}(F_0)$ are constructed to generate a pseudo null distribution which is used to estimate the level α cut-off. The maximum of all the level α cut-offs so obtained, one for each sampled mixing proportion, is then used to calibrate the TRUH statistic.

Our algorithm leverages the fact that in our virology example the number m of uninfected samples is much larger than the size n of the infected samples. Therefore, we can use the prediction strength approach of [Tibshirani and Walther \(2005\)](#) on the uninfected samples to obtain an estimate \hat{K} of the unknown number of heterogeneous subgroups K . We then use this value of \hat{K} to estimate the class memberships of the baseline samples \mathbf{U}_m using a \hat{K} -means algorithm. For $1 \leq a \leq \hat{K}$, denote by $\hat{J}_a \subseteq \{1, 2, \dots, m\}$ the subset of indices which belong to class a in the output of the \hat{K} -means algorithm. Let $U_{\hat{J}_a} = \{U_i : i \in \hat{J}_a\}$ be the subset of the baseline samples estimated to be in the a^{th} class by the \hat{K} -means algorithm. Note that $\mathbf{U}_m = \{U_{\hat{J}_a} : a = 1, 2, \dots, \hat{K}\}$ and $\sum_{a=1}^{\hat{K}} m_a = m$, where $m_a = |\hat{J}_a|$.

Now, for each $b_1 = 1, \dots, B_1$, denote by $(\lambda_1^{(b_1)}, \dots, \lambda_{\hat{K}}^{(b_1)})$ a random sample from the \hat{K} -dimensional simplex $\mathcal{S}_{\hat{K}} = \{(z_1, \dots, z_{\hat{K}}) \in \mathbb{R}^{\hat{K}} : z_a \in [0, 1], \text{ for } 1 \leq a \leq \hat{K}, \text{ and } \sum_{a=1}^{\hat{K}} z_a = 1\}$. Given the mixing weights $\{\lambda_1^{(b_1)}, \dots, \lambda_{\hat{K}}^{(b_1)}\}$, we construct B_2 surrogate infected samples from $\mathcal{F}(F_0)$ as follows: for each $b_2 = 1, \dots, B_2$ and for $1 \leq a \leq \hat{K}$, randomly sample $\lceil n\lambda_a^{(b_1)} \rceil$ elements without replacement from $U_{\hat{J}_a}$. Denote the chosen elements by

$$\mathcal{V}_a^{(b_2)} = \{U_1^{(b_2)}, \dots, U_{\lceil n\lambda_a^{(b_1)} \rceil}^{(b_2)}\},$$

and set the remaining $m_a - \lceil n\lambda_a^{(b_1)} \rceil$ elements in $U_{\hat{J}_a}$ as the residual baseline sample $\mathcal{U}_a^{(b_2)}$ in class a . Now, combining the samples over the \hat{K} classes, we get the surrogate infected sample as $\mathbf{V}_n^{(b_2)} = \{\mathcal{V}_a^{(b_2)} : a = 1, \dots, \hat{K}\}$ and the corresponding baseline sample as $\mathbf{U}_{\tilde{m}}^{(b_2)} = \{\mathcal{U}_a^{(b_2)} : a = 1, \dots, \hat{K}\}$, where

$$\tilde{m} = \sum_{a=1}^{\hat{K}} (m_a - \lceil n\lambda_a^{(b_1)} \rceil).$$

Note that under the null hypothesis of no remodeling ($G \in \mathcal{F}(F_0)$), the bootstrapped samples in the b_2^{th} round, $\mathbf{U}_{\tilde{m}}^{(b_2)}$ and $\mathbf{V}_n^{(b_2)}$ (which are surrogates for \mathbf{U}_m and \mathbf{V}_n , respectively), can be used to compute the statistic

$$T_{\tilde{m},n}^{(b_2)} = n^{\frac{1}{d}} |\tau_{fc} \cdot \bar{D}_{\tilde{m},n} - \bar{C}_{\tilde{m},n}|. \quad (8)$$

For b_1 fixed, $T_{\tilde{m},n}^{(b_2)}$ is the surrogate of the TRUH statistic in the b_2^{th} bootstrap round. Observe that compared to (7), we have introduced a tuning parameter τ_{fc} in (8) above. We define it as the fold change (fc) hyper-parameter and will consider values of $\tau_{fc} \geq 1$. Biologically relevant remodeling corresponds to significant fold change increase or decrease in the magnitude of cellular expressions between the infected and the uninfected cells. As we test the global null hypothesis of no change in any of the concerned genes, alternative hypothesis of remodeling with meager fold changes, if accepted, will only lead to biologically

uninteresting discoveries. For discovering virologically interesting alternatives, it is natural to set τ_{fc} slightly larger than 1. (Note that $\tau_{fc} = 1$ corresponds to the bootstrapped version of the TRUH statistic in (7).) In the simulation experiments presented later in Section 3 we set $\tau_{fc} = 1$ whereas in Section 4 τ_{fc} is fixed at 1.1 as we study a real-world virology dataset.

Algorithm 1: Bootstrap cut-off for a level α test using $T_{m,n}$

Input: The parameters n, τ_{fc} , and α . The baseline sample U_m , and the estimates \hat{K} and $\{\hat{J}_a : a = 1, \dots, \hat{K}\}$ from the K -means algorithm.

Output: The bootstrapped level α cutoff $t_{m,n,\alpha}$.

for $b_1 = 1, \dots, B_1$ **do**

 STEP 1: Random sample $\{\lambda_1^{(b_1)}, \dots, \lambda_{\hat{K}}^{(b_1)}\}$ from the \hat{K} -dimensional simplex;

for $b_2 = 1, \dots, B_2$ **do**

for $a = 1, \dots, \hat{K}$ **do**

if $\lceil n\lambda_a^{(b_1)} \rceil \leq m_a$ **then**

 STEP 2: Draw a simple random sample $\mathcal{V}_a^{(b_2)} = \{U_1^{(b_2)}, \dots, U_{\lceil n\lambda_a^{(b_1)} \rceil}^{(b_2)}\}$ without replacement from $U_{\hat{J}_a}$;

 STEP 3: $\mathcal{U}_a^{(b_2)} = U_{\hat{J}_a} \setminus \mathcal{V}_a^{(b_2)}$ the baseline residual sample in class a ;

else

 Stop: Go to STEP 1;

 Surrogate Case sample: $\mathbf{V}_n^{(b_2)} = \{\mathcal{V}_a^{(b_2)} : a = 1, \dots, \hat{K}\}$;

 Baseline sample: $\mathbf{U}_{\hat{m}}^{(b_2)} = \{\mathcal{U}_a^{(b_2)} : a = 1, \dots, \hat{K}\}$;

 STEP 4: Calculate $T_{\hat{m},n}^{(b_2)} = n^{\frac{1}{d}} |\tau_{fc} \bar{D}_{\hat{m},n} - \bar{C}_{\hat{m},n}|$;

 STEP 5: Return $t_{m,n,\alpha}^{(b_1)} = \min\{T_{\hat{m},n}^{(b_2)} : \frac{1}{B_2} \sum_{r=1}^{B_2} \mathbf{1}\{T_{\hat{m},n}^{(r)} \geq T_{\hat{m},n}^{(b_2)}\} \leq \alpha\}$.

STEP 6: Return $t_{m,n,\alpha} = \max\{t_{m,n,\alpha}^{(b_1)} : 1 \leq b_1 \leq B_1\}$.

The bootstrap procedure described above is summarized in Algorithm 1. The computational complexity of Algorithm 1 is driven by the following two steps: (i) the computation of the estimated number of clusters \hat{K} , and (ii) the computation of the TRUH test statistic over the bootstrap samples. While the calculations in step (ii) can be distributed across the $B_1 B_2$ bootstrap samples and n infected samples, the computational cost of estimating $T_{\hat{m},n}^{(b)}$ for a fixed b is $O(md)$ which is the cost of running the 1-nearest neighbor algorithm twice for each of the n infected samples. To estimate K , we use prediction strength along with a K -means algorithm where the target number of clusters and the maximum number of iterations over which the K -means algorithm runs before stopping are both fixed and thus has $O(md)$ complexity. Therefore the overall computational complexity of Algorithm 1 is $O(md)$. For the numerical experiments and real data analysis of Sections 3 and 4, we set $B_2 = 200$ and implement a version of Algorithm 1 which samples the mixing proportions $\{\lambda_1, \dots, \lambda_{\hat{K}}\}$ only from the corners of the \hat{K} dimensional simplex $\mathcal{S}_{\hat{K}}$ as follows: we set $B_1 = \hat{K}$ and for $b_1 = 1, \dots, B_1$, and $a = 1, \dots, \hat{K}$, we take $\lambda_a^{(b_1)} = 1$ if $b_1 = a$ and 0 otherwise. This sampling scheme ensures that the mechanism for generating

the mixing proportions places most weight on the corners of $\mathcal{S}_{\hat{K}}$.

3 Numerical Experiments

In this section we evaluate the numerical performance of the TRUH procedure across a wide range of simulation experiments. We consider the following six competing testing procedures that use different methodologies to conduct a nonparametric two-sample test: (i) Energy test (`Energy`) of [Aslan and Zech \(2005\)](#) available from the R package `energy`, (ii) Cross-Match test (`Crossmatch`) of [Rosenbaum \(2005\)](#) available from the R package `crossmatch`, (iii) edgcount test (`E_Count`) of [Friedman and Rafsky \(1979\)](#), (iv) Generalized edgcount test (`GE_Count`) of [Chen and Friedman \(2017\)](#), (v) Weighted edgcount test (`WE_Count`) of [Chen et al. \(2018\)](#), and (vi) the Max Type edgcount test (`MTE_Count`) of [Zhang and Chen \(2017\)](#). The aforementioned four edge count based tests are available from the R package `gtests`. We note that the preceding six testing procedures are not designed to test the composite null hypothesis of equation (3) and rely on a simple null hypothesis $H_0 : F_0 = G$ for inference. Nevertheless, the simulation experiments presented in this section highlight the incorrect inference that may result when traditional two-sample tests are used for testing the composite null hypothesis of equation (3).

To assess the performance of the competing testing procedures, we simulate U_m and V_n from F_0 and G , the cdf of the baseline and the infected population respectively, and for each testing procedure, we measure the proportion of rejections across 100 repetitions of the composite null hypothesis test described in (3) at 5% level of significance. For TRUH, we use Algorithm 1 with fold change constant $\tau_{fc} = 1$, $B_2 = 200$ and sample the mixing proportions only from the corners of \hat{K} dimensional simplex $\mathcal{S}_{\hat{K}}$ as described in section 2.3. The R code that reproduces our simulation results can be downloaded from the following link: https://github.com/trambakbanerjee/TRUH_paper and the associated R package is available at <https://github.com/trambakbanerjee/TRUH>.

3.1 Experiment 1

In the setup of experiment 1, we consider testing $H_0 : G \in \mathcal{F}(F_0)$ versus $H_A : G \notin \mathcal{F}(F_0)$, when F_0 is the cdf of a d dimensional Gaussian mixture distribution with three components:

$$F_0 = 0.3\mathcal{N}_d(\boldsymbol{\mu}_1, \boldsymbol{\Sigma}_1) + 0.3\mathcal{N}_d(\boldsymbol{\mu}_2, \boldsymbol{\Sigma}_2) + 0.4\mathcal{N}_d(\boldsymbol{\mu}_3, \boldsymbol{\Sigma}_3),$$

where $\boldsymbol{\mu}_1 = \mathbf{0}_d$, $\boldsymbol{\mu}_2 = -3\mathbf{1}_d$, $\boldsymbol{\mu}_3 = -\boldsymbol{\mu}_2$, and $\boldsymbol{\Sigma}_K$, for $K = 1, 2, 3$, are d dimensional positive definite matrices with eigenvalues randomly generated from the interval $[1, 10]$. To simulate \mathbf{V}_n from G , we consider two scenarios as follows:

- Scenario I: Here, $G = 0.1\mathcal{N}_d(\boldsymbol{\mu}_1, \boldsymbol{\Sigma}_1) + 0.1\mathcal{N}_d(\boldsymbol{\mu}_2, \boldsymbol{\Sigma}_2) + 0.8\mathcal{N}_d(\boldsymbol{\mu}_3, \boldsymbol{\Sigma}_3)$. In this case, G has all the subpopulations present in F_0 but at different proportions. Thus, $G \in \mathcal{F}(F_0)$, and the correct inference here is no remodeling.
- Scenario II: This setting presents a scenario where $G \notin \mathcal{F}(F_0)$ and the composite null H_0 is not true. Here, we consider $G = 0.5\mathcal{N}_d(\boldsymbol{\mu}_1, \boldsymbol{\Sigma}_1) + 0.5\mathcal{N}_d(\boldsymbol{\mu}_4, \boldsymbol{\Sigma}_4)$, where $\boldsymbol{\Sigma}_4$ is a d dimensional positive definite matrix generated independently of $\boldsymbol{\Sigma}_1, \boldsymbol{\Sigma}_2, \boldsymbol{\Sigma}_3$, and $\boldsymbol{\mu}_4 = 4\boldsymbol{\epsilon}_d$, where $\boldsymbol{\epsilon}_d$ is a vector of d independent Rademacher random variables.

Table 2: Rejection rates at 5% level of significance: Experiment 1 and Scenario I wherein $H_0 : G \in \mathcal{F}(F_0)$ is true.

Method	$m = 500, n = 50$			$m = 2000, n = 200$		
	$d = 5$	$d = 15$	$d = 30$	$d = 5$	$d = 15$	$d = 30$
Energy	1.000	1.000	1.000	1.000	1.000	1.000
Crossmatch	0.220	0.150	0.145	0.460	0.410	0.340
E Count	0.185	0.115	0.055	0.400	0.335	0.195
GE Count	0.170	0.185	0.225	0.510	0.540	0.605
WE Count	0.300	0.295	0.360	0.655	0.745	0.735
MTE Count	0.230	0.230	0.290	0.605	0.665	0.665
TRUH	0.02	0.015	0.015	0.01	0.02	0.01

For scenario I, table 2 reports the rejection rates for 100 repetitions of the test for varying d, m, n when the parameters $\{\boldsymbol{\mu}_i, \boldsymbol{\Sigma}_i \mid 1 \leq i \leq 4\}$ are held fixed across these repetitions. We see that TRUH returns the smallest rejection rate. The other six tests all have very high rejection rates as they fail to account for the composite nature of the null hypothesis. The rejection rate for TRUH is below the prespecified 0.05 level establishing that it is a conservative test across all the regimes considered in the table. In scenario II, however, we find that all the tests correctly identify $G \notin \mathcal{F}(F_0)$ in all the regimes and across all replications. This shows, all the tests exhibit perfect rejection rates in this scenario. These two scenarios under experiment 1 demonstrate that for testing the composite null hypothesis of equation (3), direct application of traditional two-sample tests such as those considered here, is no longer conservative as these tests rely on a simple null hypothesis for inference. TRUH, on the other hand, is adept at detecting $H_0 : G \in \mathcal{F}(F_0)$ and powerful against departures from H_0 .

In Table 3 we present the results of the simulation exercise that correspond to the three scenarios described in figure 3. The two dimensional uninfected marker expressions (X_1, X_2) are randomly sampled from $F_0 = w_1\mathcal{N}_2(\boldsymbol{\mu}_1, \mathbf{I}_2) + w_2\mathcal{N}_2(\boldsymbol{\mu}_2, \mathbf{I}_2) + w_3\mathcal{N}_2(\boldsymbol{\mu}_3, \mathbf{I}_2)$, where $\boldsymbol{\mu}_1 = \mathbf{0}$, $\boldsymbol{\mu}_2 = (0, -4)$, $\boldsymbol{\mu}_3 =$

Table 3: Rejection rates at 5% level of significance: Simulation experiment corresponding to Figure 3.

Method	$m = 2000, n = 500, d = 2$		
	Left panel:	Center panel:	Right panel:
	no remodeling ($G \in \mathcal{F}(F_0)$)	remodeling ($G \notin \mathcal{F}(F_0)$)	preferential infection ($G \in \mathcal{F}(F_0)$)
Energy	0.030	1.000	1.000
Crossmatch	0.030	1.000	1.000
E Count	0.010	1.000	1.000
GE Count	0.000	1.000	1.000
WE Count	0.060	1.000	1.000
MTE Count	0.030	1.000	1.000
TRUH	0.000	0.980	0.000

$(4, -2)$ and the sample size is $m = 2000$. The mixing weights are given by $(w_1, w_2, w_3) = (0.3, 0.3, 0.4)$. For the panel on the left of figure 3, infected marker expressions arise from F_0 but with sample size $n = 500$, while for the center panel the infected marker expressions represent a random sample of size n from $G = 0.5\mathcal{N}_2(\boldsymbol{\mu}_4, \mathbf{I}_2) + 0.5\mathcal{N}_2(\boldsymbol{\mu}_5, \mathbf{I}_2)$, where $\boldsymbol{\mu}_4 = 0.25\boldsymbol{\mu}_2 + 0.5\boldsymbol{\mu}_3$ and $\boldsymbol{\mu}_5 = (3/4)\boldsymbol{\mu}_2 + (9/8)\boldsymbol{\mu}_3$. Clearly in this case $G \notin \mathcal{F}(F_0)$. For the right most panel, infected marker expressions are again a random sample of size n from $\mathcal{F}(F_0)$ with mixing weights given by the vector $(w_1, w_2, w_3) = (0.8, 0.1, 0.1)$. Under this setting, the three g-tests (Chen et al., 2018, Chen and Friedman, 2017, Friedman and Rafsky, 1979), the cross-match test of Rosenbaum (2005), and the energy test of Aslan and Zech (2005) infer $G \notin \mathcal{F}(F_0)$ in all of the 100 repetitions of the experiment thus suggesting their inability to tackle subpopulation level heterogeneity.

3.2 Experiment 2

For experiment 2, we consider a more complex setup wherein F_0 is the cdf of a d dimensional mixture distribution which is not necessarily Gaussian. Here,

$$F_0 = 0.5 \text{Gam}_d(\text{shape} = 5\mathbf{1}_d, \text{rate} = \mathbf{1}_d, \boldsymbol{\Sigma}_1) + 0.5 \text{Exp}_d(\text{rate} = \mathbf{1}_d, \boldsymbol{\Sigma}_2),$$

where Gam_d and Exp_d are d dimensional Gamma and Exponential distributions. For generating correlated Gamma and Exponential variables, we use the Gaussian copula approach based function from the R-package `lcmix` (Dvorkin, 2012, Xue-Kun Song, 2000). We consider tapering matrices with positive and negative autocorrelations: $(\boldsymbol{\Sigma}_1)_{ij} = 0.7^{|i-j|}$ and $(\boldsymbol{\Sigma}_2)_{ij} = -0.9^{|i-j|}$ for $1 \leq i, j \leq d$. For simulating \mathbf{V}_n from G , we consider the following two scenarios:

- Scenario I: Here, $G = \text{Exp}_d(\text{rate} = \mathbf{1}_d, \boldsymbol{\Sigma}_2)$. In this case, G arises from only one of the components of F_0 , that is, $G \in \mathcal{F}(F_0)$.
- Scenario II: Here, $G = 0.1 \text{Gam}_d(\text{shape} = 10\mathbf{1}_d, \text{rate} = 0.5\mathbf{1}_d, \boldsymbol{\Sigma}_1) + 0.9 \text{Exp}_d(\text{rate} = \mathbf{1}_d, \boldsymbol{\Sigma}_2)$. In this setting, $G \notin \mathcal{F}(F_0)$ and the composite null H_0 is not true. When the ratio n/m is small,

this scenario presents a difficult setting for detecting departures from H_0 as majority of the case samples from V_n will arise from $\text{Exp}_d(\text{rate} = \mathbf{1}_d, \Sigma_2)$ and the tests will rely on only a small fraction of samples from $\text{Gam}_d(\text{shape} = 10\mathbf{1}_d, \text{rate} = 0.5\mathbf{1}_d, \Sigma_1)$ to reject the null hypothesis.

Table 4: Rejection rates at 5% level of significance: Experiment 2 and Scenario I wherein $H_0 : G \in \mathcal{F}(F_0)$ is true.

Method	$m = 500, n = 50$			$m = 2000, n = 200$		
	$d = 5$	$d = 15$	$d = 30$	$d = 5$	$d = 15$	$d = 30$
Energy	1.000	1.000	1.000	1.000	1.000	1.000
Crossmatch	0.460	0.440	0.390	0.800	0.850	0.760
E Count	0.290	0.190	0.280	0.720	0.690	0.560
GE Count	0.400	0.430	0.390	0.900	0.920	0.900
WE Count	0.560	0.590	0.600	0.970	0.960	0.940
MTE Count	0.460	0.510	0.440	0.930	0.950	0.910
TRUH	0.000	0.000	0.000	0.000	0.000	0.000

Table 5: Rejection rates at 5% level of significance: Experiment 2 and Scenario II wherein $H_0 : G \in \mathcal{F}(F_0)$ is false.

Method	$m = 500, n = 10$			$m = 2000, n = 40$		
	$d = 5$	$d = 15$	$d = 30$	$d = 5$	$d = 15$	$d = 30$
Energy	0.930	0.960	1.000	1.000	1.000	1.000
Crossmatch	0.400	0.350	0.470	0.600	0.720	0.720
E Count	0.180	0.120	0.130	0.340	0.310	0.200
GE Count	0.310	0.230	0.160	0.800	0.790	0.770
WE Count	0.510	0.490	0.460	0.800	0.790	0.790
MTE Count	0.390	0.430	0.380	0.800	0.780	0.770
TRUH	0.580	0.580	0.580	0.880	0.940	0.960

Table 4 reports the rejection rates, for 100 repetitions, of the different tests in scenario I. Note that TRUH correctly identifies that $G \in \mathcal{F}(F_0)$ while the remaining tests overwhelmingly support $G \notin \mathcal{F}(F_0)$, especially when m is large, demonstrating their lack of conservatism in testing the composite null hypothesis of the form (3). The results for scenario II (Table 5) are reported for $n/m = 0.02$, where, with the exception of Energy test, all the other competing tests demonstrate small rejection rates for $m = 500$. Substantial improvement in the rejection rates is evident when $m = 2000$. However, for both these cases, $m = 500$ and $m = 2000$, the Energy test followed by TRUH exhibit the largest rejection rates. Although Energy test rejects H_0 in almost all of the testing instances in scenario II, its performance in scenario I (Table 4) reveals that it can be severely non-conservative when testing under a composite null hypothesis $H_0 : G \in \mathcal{F}(F_0)$.

3.3 Experiment 3

For experiment 3, we introduce zero inflation in both the baseline and case samples to mimic the scenario that is often encountered in virology studies wherein some of the markers exhibit only a small probability of expressing themselves. We let $\mathbf{p} = (p_1, \dots, p_d)$ denote the d dimensional vector of point masses at 0 across dimensions, and consider

$$F_0 = 0.5F_1 + 0.5F_2,$$

where $F_1 = \mathbf{p}\delta_{\{0\}} + (\mathbf{1}_d - \mathbf{p}) \text{Gam}_d(\text{shape} = 5\mathbf{1}_d, \text{rate} = \mathbf{1}_d, \Sigma_1)$ and $F_2 = \mathbf{p}\delta_{\{0\}} + (\mathbf{1}_d - \mathbf{p}) \text{Exp}_d(\text{rate} = \mathbf{1}_d, \Sigma_2)$. In the above representation, \mathbf{p} regulates the differential zero inflation across the d dimensions. For the purposes of this experiment, we chose the first $0.8d$ coordinates of \mathbf{p} independently from $\text{Unif}(0.5, 0.6)$, and the remaining $0.2d$ coordinates are set to 0. Thus, the zero inflation is encountered only in the first $0.8d$ coordinates of F_0 . To simulate the baseline sample U_m from F_0 , we use the R-package `lcmix` with Σ_1, Σ_2 as described in experiment 2 (Section 3.2). For simulating V_n from G , we consider the following two scenarios:

- Scenario I: Let $G = \mathbf{p}\delta_{\{0\}} + (\mathbf{1}_d - \mathbf{p}) \text{Exp}_d(\text{rate} = \mathbf{1}_d, \Sigma_2)$. Here, G arises from only one of the components of F_0 , that is, $G \in \mathcal{F}(F_0)$.
- Scenario II: Here, we let $G = 0.5G_1 + 0.5G_2$, where $G_1 = \mathbf{q}\delta_{\{0\}} + (\mathbf{1}_d - \mathbf{q}) \text{Gam}_d(\text{shape} = 5\mathbf{1}_d, \text{rate} = 0.5\mathbf{1}_d, \Sigma_1)$ and $G_2 = \mathbf{q}\delta_{\{0\}} + (\mathbf{1}_d - \mathbf{q}) \text{Exp}_d(\text{rate} = \mathbf{1}_d, \Sigma_2)$, and we set the first $0.8d$ coordinates of \mathbf{q} to 0.3 and the remaining $0.2d$ coordinates to 0. Note that in this setting, apart from the difference in the rate parameter of the Gamma distribution, we also have differential zero inflation across G and F_0 , as $\mathbf{q} \neq \mathbf{p}$. Thus, $G \notin \mathcal{F}(F_0)$ and the composite null H_0 is not true. Moreover, when n is small, this scenario presents a challenging setting for detecting departures from H_0 as the tests will have to rely on both the differences in the rate parameter and differential zero expression between U_m, V_n to reject the null hypothesis.

Table 6: Rejection rates at 5% level of significance: Experiment 3 and Scenario I wherein $H_0 : G \in \mathcal{F}(F_0)$ is true.

Method	$m = 500, n = 50$			$m = 2000, n = 200$		
	$d = 5$	$d = 15$	$d = 30$	$d = 5$	$d = 15$	$d = 30$
Energy	1.000	1.000	1.000	1.000	1.000	1.000
Crossmatch	0.340	0.330	0.240	0.730	0.800	0.670
E Count	0.200	0.120	0.100	0.670	0.440	0.340
GE Count	0.300	0.290	0.330	0.870	0.860	0.870
WE Count	0.510	0.460	0.540	0.970	0.920	0.930
MTE Count	0.400	0.350	0.460	0.890	0.910	0.920
TRUH	0.000	0.000	0.000	0.000	0.000	0.000

Table 7: Rejection rates at 5% level of significance: Experiment 3 and Scenario II wherein $H_0 : G \in \mathcal{F}(F_0)$ is false.

Method	$m = 500, n = 10$			$m = 2000, n = 40$		
	$d = 5$	$d = 15$	$d = 30$	$d = 5$	$d = 15$	$d = 30$
Energy	0.850	0.920	0.940	1.000	1.000	1.000
Crossmatch	0.460	0.410	0.590	0.820	0.730	0.970
E Count	0.410	0.520	0.730	0.890	0.990	1.000
GE Count	0.410	0.480	0.730	0.920	0.960	1.000
WE Count	0.550	0.580	0.780	0.920	0.920	1.000
MTE Count	0.590	0.570	0.810	0.900	0.960	1.000
TRUH	0.760	0.940	0.980	0.970	1.000	1.000

Tables 6 and 7 report the rejection rates for 100 repetitions of the test when p is held fixed across these repetitions. For scenario I (Table 6), we see that TRUH, unlike the other six tests, does not excessively reject the null hypothesis and is the only conservative test. In scenario II (Table 7) when $n = 10$, the TRUH and Energy tests dominate all the remaining tests and reject H_0 in more than 80% of the testing instances. However when $n = 40$, all tests are competitive, with the exception of the Crossmatch for $d < 30$. Overall, across the above two zero-inflated scenarios, TRUH is both conservative and powerful against departures from the null hypothesis $H_0 : G \in \mathcal{F}(F_0)$.

4 Remodeling Analysis of HIV-Infected T Cells

In this section, we analyze the data collected in Cavrois et al. (2017). It contains protein expressions of uninfected and HIV infected CD4 (which is a protein found on the surface of immune cells) positive tonsillar T cells. We show that existing two-sample tests that rely on a simple null hypothesis for inference, may lead to biologically incorrect inference when testing the composite null hypothesis of equation (3). Our proposed TRUH hypothesis testing framework, on the other hand, is proficient at detecting $H_0 : G \in \mathcal{F}(F_0)$ and powerful against departures from H_0 .

As discussed in section 1.1, the goal in Cavrois et al. (2017) was to conduct a mass cytometric assessment of subsets of CD4+ T cells that support HIV entry and viral infection in humans using two variants of the HIV virus: *Nef rich* HIV and *Nef deficient* HIV. It is known in the immunology literature, that *Nef-rich* cells are more prone to viral remodeling (Basmaciogullari and Pizzato, 2014). The data set we analyze here contains uninfected and infected data from two different sets of experiments. Both the experiments have four replications based on tonsillar T cells from 4 healthy donors. In Experiment I, the infection was done by *Nef-rich* HIV where as in Experiment II the infection was done by *Nef-deficient* HIV. We expect remodeling, if any, in the infected cells to be higher in experiment I than in experiment II compared to their respective baseline uninfected populations.

The cells in the data were phenotyped in a 38 parameter CyToF (Bendall et al., 2014) panel after allowing 4 days for infection. The panel used 3 markers to classify the cells as uninfected or infected which leaves $d = 35$ of the original 38 markers for our analyses. For donor r , let $\mathbf{U}_{m,r} = \{U_{1,r}, \dots, U_{m,r}\}$ denote the uninfected sample where each $U_{j,r}$ is a d dimensional vector of arcsin transformed marker expression values with cdf F_0 . We assume that the heterogeneity in the uninfected population is captured by K heterogeneous cellular subgroups each having unimodal probability distribution functions with cdfs F_1, F_2, \dots, F_K and mixing proportions w_1, w_2, \dots, w_K , such that F_0 is of the form represented in equation (1). We observe the virus infected sample $\mathbf{V}_{n,r} = \{V_{1,r}, \dots, V_{n,r}\}$ consisting of n i.i.d. d -dimensional arcsin transformed observations from G and the goal is to test $H_0 : G \in \mathcal{F}(F_0)$ versus $H_A : G \notin \mathcal{F}(F_0)$, where $\mathcal{F}(F_0)$ is the convex hull of $\{F_1, \dots, F_K\}$ as defined in equation (2). Note that rejection of the null hypothesis would indicate that the distribution of the marker expressions under infection is different from F_0 and any convex combination of its components, thus providing evidence in favor of remodeling. Virologist study remodeling in virus infected cells in reference to the expressions of Bystander cells. In panels of cells subjected to infection by the virus, not all the cells get infected. Bystanders are those cells which are not directly infected by the virus but are neighbors of virus infected cells. In these experiments, it was seen that when τ_{fc} is set to 1 then even Bystander cells exhibit remodeling in some experiments. However, when τ_{fc} is set to 1.1, there is no remodeling in the Bystander population in any experiments. Thus, to detect biologically relevant cases of remodeling and avoid discovering benign instances, we use $\tau_{fc} = 1.1$ through out this section to obtain the bootstrapped null distribution of the TRUH statistic.

Among the 35 markers considered here, it is known that the expressions of the four markers CD4, CCR5, CD28, and CD62L are changed due to HIV infection and these four markers play a significant role in HIV induced remodeling (Garcia and Miller, 1991, Matheson et al., 2015, Michel et al., 2005, Ross et al., 1999, Swigut et al., 2001, Vassena et al., 2015). Consider two testing problems: (A) in which we test the hypothesis for all 35 markers, and (B) in which we test the hypothesis of viral remodeling on 31 markers leaving aside the four markers which are known to be remodeled by HIV. Thus, here we have four different cases on which we conduct the tests of viral remodeling, viz.,

- CASE 1 corresponds to Experiment I A where we test viral remodeling on `Nef-rich` infected cells based on all 35 markers including the four which are known to be remodeled.
- CASE 2 corresponds to Experiment I B where we test viral remodeling on `Nef-rich` infected cells based on 31 markers which are known to be mainly invariant under HIV infection.
- CASE 3 corresponds to Experiment II A where we test viral remodeling on `Nef-deficient`

infected cells based on all 35 markers including the four which are known to be remodeled.

- CASE 4 corresponds to Experiment II B where we test viral remodeling on *Nef*-deficient infected cells based on 31 markers which are known to be mainly invariant under HIV infection.

In all the four cases, we have four replications corresponding to four donors. It has been established through validation experiments in [Cavrois et al. \(2017\)](#) that there is no remodeling but only preferential infection in cases 2 and 4 whereas cases 1 and 3 exhibits remodeling with the intensity of remodeling being much higher in the former than the later. Biologically, it corresponds to the fact that there is *Nef*-independent remodeling but the intensity of remodeling is higher in presence of *Nef*. Also, remodeling in cellular expressions is confined to the four markers CD4, CCR5, CD28, and CD62L in the set of markers considered in the study. Figures 7 and 8 present t-SNE plots ([Maaten and Hinton, 2008](#)) of the data where the d dimensional uninfected and infected cellular expression levels are projected to a two dimensional space for each of the four donors across the four cases. While these plots exhibit the underlying heterogeneity in the uninfected sample and the sample size imbalance, instances of remodeling are also visible in cases 1 and 3 (figure 7) wherein a relatively large fraction of the infected cells in red occupy a distinct position in the two dimensional space with no overlap with their uninfected counterparts.

For conducting statistical hypothesis test for the above four cases, along with our proposed TRUH procedure, we also use the six other competing tests statistics described in section 3 which are the

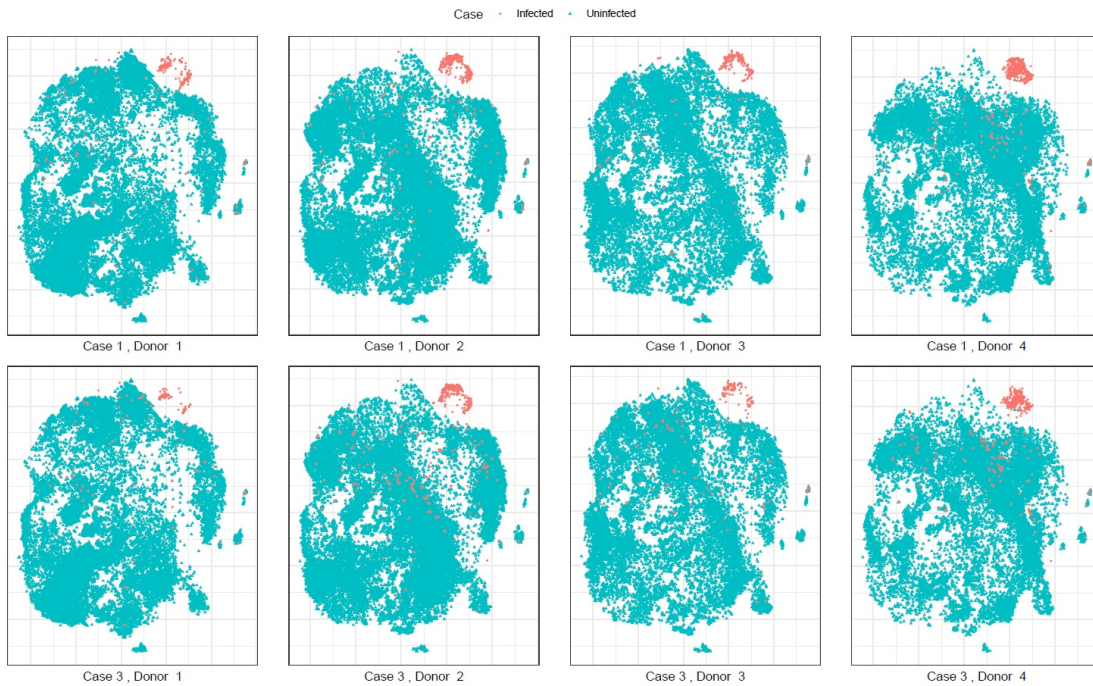


Figure 7: This is a t-SNE plot ([Maaten and Hinton, 2008](#)) of the data for Cases 1 and 3 where the $d = 35$ dimensional uninfected and infected cellular expression levels are projected to a two dimensional space for each of the four donors.

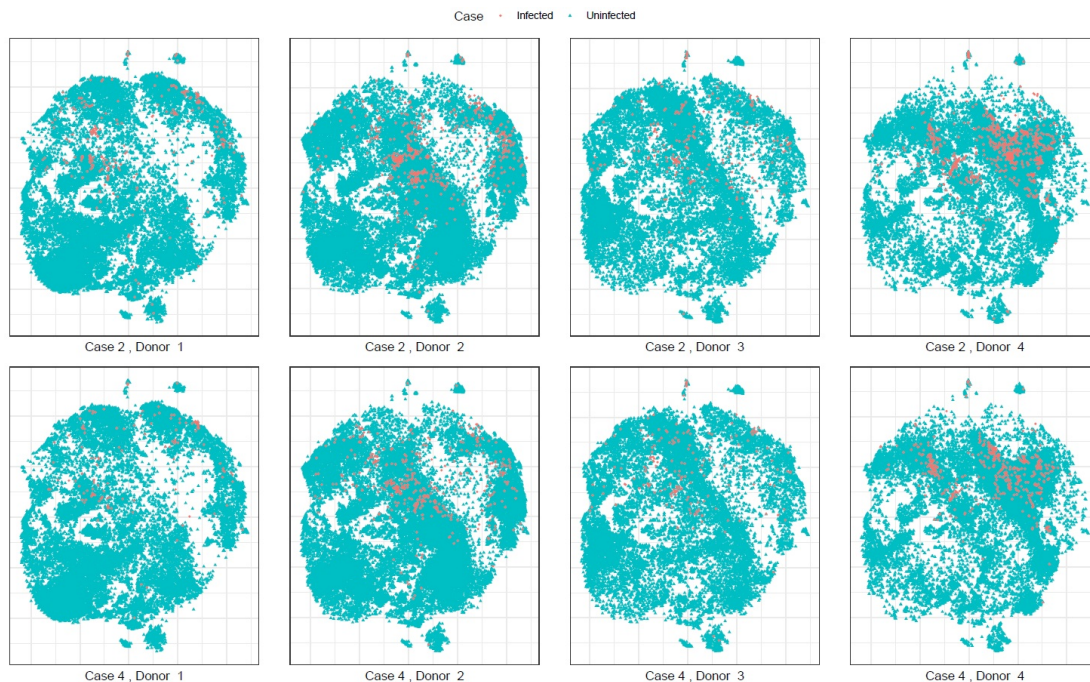


Figure 8: This is a t-SNE plot of the data for Cases 2 and 4 where the $d = 31$ dimensional uninfected and infected cellular expression levels are projected to a two dimensional space for each of the four donors.

Energy test (Aslan and Zech, 2005), CrossMatch (Rosenbaum, 2005), E Count (Friedman and Rafsky, 1979), GE Count (Chen and Friedman, 2017), WE Count (Chen et al., 2018) and MTE Count (Zhang and Chen, 2017). As discussed in section 3 these six testing procedures are not designed to test the composite null hypothesis of equation (3) and rely on a simple null hypothesis $H_0 : F_0 = G$ for inference. In this section we highlight the biologically incorrect inference that may result when these tests are used for testing the composite null hypothesis of no remodeling.

Figure 9 presents the values of the TRUH statistic and the 2.5-th, 50-th, 97.5-th percentiles of the associated null distribution. From the plots, it is evident that at 5% level our proposed procedure correctly captures the biological phenomena of remodeling or no remodeling across the four cases. The other six tests fail to correctly detect the phenomena in some of the four cases due to heterogeneity in the data. Next, we describe the results in further details. In Tables 8 and 9 we report the p-values of the seven competing tests statistics for testing remodeling under HIV infection in *Nef*-rich environment. In Table 8 all seven tests reject the null hypothesis of no remodeling, thus verifying that CD4+ T cells exhibit remodeling under the influence of *Nef* rich HIV infection. In Table 9, however, we present the p-values of the tests when the four cell surface markers, CD4, CCR5, CD28, and CD62L, known to be down regulated by *Nef*, were removed from our analysis ($d = 31$). Other than donor 1, TRUH indicates no remodeling in this scenario for the remaining three donors which is expected given the mechanism

of remodeling that Nef pursues by down-regulating CD4, CCR5, CD28, and CD62L (Swigut et al., 2001). The absence of these four cell markers from the uninfected and infected samples reduces the phenotypic gap between these samples as measured through their surface markers. The top row in Figure 9 shows that while the null distribution shifts down from CASE 1 (left plot) to CASE 2 (right plot) across all four donors, the drop in the magnitude of the TRUH statistic is far more substantial when the four surface markers are excluded. The remaining six test statistics appear to be insensitive to these subtle changes in the uninfected and infected samples across the two scenarios and, continue to detect remodeling in Case 2 which is actually no remodeling but preferential infection. This demonstrates their inability to handle heterogeneity in the data that TRUH tackles via the composite null testing framework of equations (1)-(3).

In Tables 10 and 11, we present the p-values of the seven test statistics for testing the null hypothesis

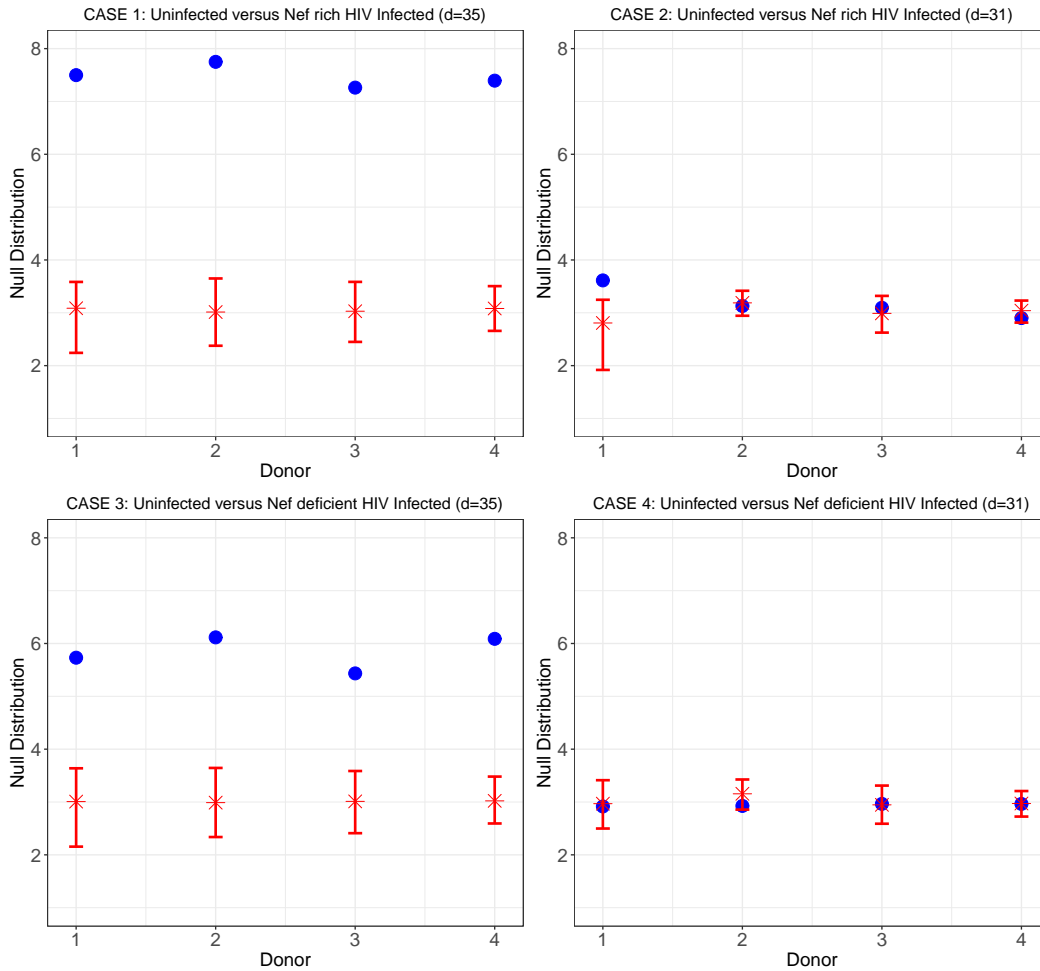


Figure 9: Null distribution of the TRUH statistic under cases 1-4. The blue dots are magnitudes of TRUH statistic for each donor under the four cases while the red bars indicate the 2.5-th, 50-th and 97.5-th percentiles of the bootstrapped null distribution obtained from algorithm 1 with $\tau_{fc} = 1.1$.

Table 8: p-values in CASE 1: Uninfected versus *Nef*-rich HIV Infected for entire 35 markers.

Tests	Donor 1 $m = 24,984, n = 245$	Donor 2 $m = 31,552, n = 521$	Donor 3 $m = 17,704, n = 211$	Donor 4 $m = 22,830, n = 660$
Energy	< 0.001	< 0.001	< 0.001	< 0.001
CrossMatch	0.005	0.005	0.005	0.005
E Count	< 0.001	< 0.001	< 0.001	< 0.001
GE Count	< 0.001	< 0.001	< 0.001	< 0.001
WE Count	< 0.001	< 0.001	< 0.001	< 0.001
MTE Count	< 0.001	< 0.001	< 0.001	< 0.001
TRUH	< 0.001	< 0.001	< 0.001	< 0.001

Table 9: p-values in CASE 2: Uninfected versus *Nef*-rich HIV Infected for 31 invariant markers.

Tests	Donor 1 $m = 24,984, n = 245$	Donor 2 $m = 31,552, n = 521$	Donor 3 $m = 17,704, n = 211$	Donor 4 $m = 22,830, n = 660$
Energy	< 0.001	< 0.001	< 0.001	< 0.001
CrossMatch	0.005	0.005	0.005	0.005
E Count	< 0.001	< 0.001	< 0.001	< 0.001
GE Count	< 0.001	< 0.001	< 0.001	< 0.001
WE Count	< 0.001	< 0.001	< 0.001	< 0.001
MTE Count	< 0.001	< 0.001	< 0.001	< 0.001
TRUH	< 0.001	0.67	0.274	0.914

H_0 of no remodeling when the HIV infected sample lacks the critical *Nef* gene (see Construction and validation of reporter viruses in Supplemental Experimental Procedures of [Cavrois et al. \(2017\)](#) for details around the generation of *Nef*-deficient HIV infected cells). We see that TRUH rejects the null hypothesis of no remodeling in CASE 3 (Table 10) while fails to do so in CASE 4 (Table 11), thus corroborating the biological phenomena that (a) *Nef* independent remodeling is prevalent in HIV infected cells and, (b) even in the absence of *Nef*, the down regulation of the four surface markers by other mechanisms contributes to remodeling. The bottom row in Figure 9 presents the values of the TRUH statistic and the 2.5-th, 50-th, 97.5-th percentiles of the associated null distribution. Similar observations from the top row continue to hold for cases 3 and 4 in the bottom row of Figure 9 wherein the drop in the magnitude of TRUH statistic is far more significant when the four surface markers are excluded. Moreover, from Figure 9, we see that for every donor the TRUH statistic obeys a rank ordering across the scenarios which is of the form $\text{TRUH}_1 > \text{TRUH}_3 > \text{TRUH}_2 > \text{TRUH}_4$ where TRUH_s is the magnitude of the TRUH statistic under cases $s = 1, \dots, 4$. This is not accidental for the relative strength of remodeling is known to be highest under the influence of *Nef*-rich HIV infection and more so when *Nef* down-regulates the four cell surface markers, CD4, CCR5, CD28, and CD62L. As was seen in cases 1 and 2, the remaining six tests continue to side in favor of remodeling in both cases 3 and 4, thus reflecting their relative lack of conservatism in detecting remodeling under our composite null testing framework.

The remodeling analysis of the HIV-infected T Cells reveals that our proposed testing procedure, TRUH, conforms to the biologically validated phenomenon of remodeling of human tonsillar T cells under both *Nef*-rich (case 1) and *Nef*-deficient (case 3) HIV infection. However unlike traditional tests

Table 10: p-values in CASE 3: Uninfected versus *Nef*-deficient HIV Infected for the entire 35 markers.

Tests	Donor 1 $m = 24,984, n = 129$	Donor 2 $m = 31,552, n = 382$	Donor 3 $m = 17,704, n = 174$	Donor 4 $m = 22,830, n = 440$
Energy	< 0.001	< 0.001	< 0.001	< 0.001
CrossMatch	0.005	0.005	0.005	0.005
E Count	< 0.001	< 0.001	< 0.001	< 0.001
GE Count	< 0.001	< 0.001	< 0.001	< 0.001
WE Count	< 0.001	< 0.001	< 0.001	< 0.001
MTE Count	< 0.001	< 0.001	< 0.001	< 0.001
TRUH	< 0.001	< 0.001	< 0.001	< 0.001

Table 11: p-values in CASE 4: Uninfected versus *Nef*-deficient HIV Infected for 31 invariant markers.

Tests	Donor 1 $m = 24,984, n = 129$	Donor 2 $m = 31,552, n = 382$	Donor 3 $m = 17,704, n = 174$	Donor 4 $m = 22,830, n = 440$
Energy	< 0.001	< 0.001	< 0.001	< 0.001
CrossMatch	0.005	0.005	0.005	0.005
E Count	< 0.001	< 0.001	< 0.001	< 0.001
GE Count	< 0.001	< 0.001	< 0.001	< 0.001
WE Count	< 0.001	< 0.001	< 0.001	< 0.001
MTE Count	< 0.001	< 0.001	< 0.001	< 0.001
TRUH	0.58	0.94	0.464	0.524

that continue to infer remodeling in cases 2 and 4, TRUH detects preferential infection and concludes that phenotypic differences between the HIV infected and uninfected T cells are primarily driven by variations in the expression levels of CD4, CCR5, CD28, and CD62L across the uninfected and infected cells. Moreover, through cases 1 and 2, TRUH corroborates the findings in [Chaudhuri et al. \(2007\)](#), [Michel et al. \(2005\)](#), [Swigut et al. \(2001\)](#), [Vassena et al. \(2015\)](#) that HIV remodeling of the T cells is driven by *Nef* dependent down-regulation of CD4, CCR5, CD28, CD62L while through cases 3 and 4 TRUH reveals *Nef* independent remodeling of T cells as evidenced in [Cavrois et al. \(2017\)](#).

5 Optimality Properties of the TRUH Statistic

In this section we derive the L_2 -limit of the proposed test statistic $T_{m,n}$ in the usual limiting regime where the sample sizes $m, n \rightarrow \infty$, such that $n/m \rightarrow \rho > 0$. This can be used to choose a cut-off and construct a test based on $T_{m,n}$, and show asymptotic consistency for biologically relevant location alternatives.

Recall, that the uninfected and infected samples are denoted as

$$\mathbf{U}_m = \{U_1, \dots, U_m\} \quad \text{and} \quad \mathbf{V}_n = \{V_1, \dots, V_n\}, \quad (9)$$

which are i.i.d. samples from two unknown densities f_0 and g in \mathbb{R}^d , respectively. To derive the limit of $T_{m,n}$ we need certain integrability/moment assumptions on f_0 and g .

Assumption 1. The densities f_0 and g have a common support $S \subseteq \mathbb{R}^d$ and satisfy either one of the following two assumptions depending on the dimension:

1. For $d \leq 2$, the support S is compact (with a non-empty interior) and f_0 and g are bounded away from zero on S .
2. For $d \geq 3$, f_0 and g satisfy the following conditions: $\int_S f_0(y)^{1-\frac{1}{d}} dy < \infty$, $\int_S f_0(y)^{-\frac{1}{d}} g(y) dy < \infty$, and $\int_S |y|^r f_0(y) dy < \infty$, $\int_S |y|^r g(y) dy < \infty$, for some $r > d/(d-2)$.

To describe the limit of $T_{m,n}$ we need a few definitions: For $\lambda > 0$, denote by \mathcal{P}_λ the homogeneous Poisson process of intensity λ in \mathbb{R}^d , and $\mathcal{P}_\lambda^x = \mathcal{P}_\lambda \cup \{x\}$, for $x \in \mathbb{R}^d$. Now, define the following two quantities:

$$\zeta_1(\mathbf{0}, \mathcal{P}_1) = \inf_{b \in \mathcal{P}_1} \|b\| \quad \text{and} \quad \zeta_2(\mathbf{0}, \mathcal{P}_1) = \inf_{b \in \mathcal{P}_1 \setminus N(\mathbf{0}, \mathcal{P}_1)} \|N(\mathbf{0}, \mathcal{P}_1) - b\|, \quad (10)$$

that is, the distance from the origin $\mathbf{0}$ in \mathbb{R}^d to its nearest neighbor in the Poisson process \mathcal{P}_1 , and the distance of this point to its neighbor in \mathcal{P}_1 , respectively.

Theorem 1. *Let $T_{m,n}$ be as in (7). Then, for f_0 and g as in Assumption 1 above, as $m, n \rightarrow \infty$ such that $n/m \rightarrow \rho$,*

$$T_{m,n} \xrightarrow{L_2} \varphi(f_0, g, \rho) = \rho^{\frac{1}{d}} \Delta_d \int \frac{g(y)}{f_0(y)^{\frac{1}{d}}} dy, \quad (11)$$

with $\Delta_d = (\zeta_2 - \zeta_1)$, where

- $\zeta_1 = \mathbb{E}\zeta_1(\mathbf{0}, \mathcal{P}_1)$, the expected distance from the origin in $\mathbf{0} \in \mathbb{R}^d$ to its nearest neighbor in \mathcal{P}_1 , and
- $\zeta_2 = \mathbb{E}\zeta_2(\mathbf{0}, \mathcal{P}_1)$, the expected distance between the nearest neighbor of the origin in \mathcal{P}_1 to its nearest neighbor in \mathcal{P}_1 .

The above theorem gives the L_2 -limit of the test statistic for general distributions f_0 and g . The proof of the theorem, which is given in the supplementary materials (Section B), uses the machinery of geometric stabilization, introduced by [Penrose and Yukich \(2003\)](#), which obtains the asymptotics of nearest neighbor based functionals in terms of functionals defined on a homogeneous Poisson process. Before we discuss how the result in Theorem 1 can be used to construct a test based on $T_{m,n}$ for the hypothesis (2), we discuss some properties and the consequences of the limit in (11):

- Note that the finiteness of the limit in (11) is ensured by Assumption 1. For $d \geq 3$, the moment conditions in Assumption 1 are required to establish the L_2 convergence in (11). This assumption can be relaxed to $\int_S |y|^r f_0(y) dy < \infty$ and $\int_S |y|^r g(y) dy < \infty$, for some $r > d/(d-1)$, if we

are only interested in L_1 convergence (by combining the proof of Theorem 1 with that of (Penrose and Yukich, 2003, Proposition 3.2)). However, this still does not apply for $d = 1$, where it is necessary to assume the compactness of the support, in order to ensure that the limit in (11) is finite. This is a well-known constraint which arises in a large family of random geometric graphs, while dealing with the asymptotics of edge-lengths (see, for example, (Penrose and Yukich, 2003, Theorem 1.1) and the references therein). Even though the compactness assumption technically rules out some natural distributions, from a practical standpoint, there is no real concern because one can approximate the univariate density by truncating it to a large interval, on which the above result applies. Incidentally, there has been recent work on relaxing the compactness and density bounded below assumptions in the related problems of nearest-neighbor classification Cannings et al. (2019), Gadat et al. (2016) and entropy estimation Berrett et al. (2019), which could provide useful insights on how to relax these assumptions from Theorem 1, and what are the effects of tail behavior on the heterogeneity testing problem.

- Note that ζ_1 and ζ_2 are both constants, which depend only on the dimension d . In fact, ζ_1 has a closed form expression which can be easily derived. To this end, denote by V_d and S_d the volume and the surface area of the unit ball in \mathbb{R}^d , respectively. It is easy to verify that $S_d = dV_d$. Moreover, for $r > 0$ and $x \in \mathbb{R}^d$, denote by $B(x, r)$ the ball of radius r centered at $x \in \mathbb{R}^d$. Then, using the observation that a point b is the nearest neighbor of the origin, if there are no points of the Poisson process \mathcal{P}_1 in the ball $B(0, \|b\|)$, it follows that

$$\zeta_1 = \mathbb{E}(\zeta_1(\mathbf{0}, \mathcal{P}_1)) = \int \|b\| \mathbb{P}(b = N(\mathbf{0}, \mathcal{P}_1^{0,b})) db = S_d \int_0^\infty t^d e^{-V_d t^d} dt,$$

which, by the change of variable $x = V_d t^d$ equals

$$\left(\frac{1}{V_d}\right)^{\frac{1}{d}} \int_0^\infty x^{\frac{1}{d}} e^{-x} dx = \left(\frac{1}{V_d}\right)^{\frac{1}{d}} \Gamma\left(\frac{d+1}{d}\right), \quad (12)$$

where $\Gamma(\cdot)$ denotes the Gamma function.

Theorem 1 shows that for K fixed densities f_1, \dots, f_K , and $f_0 = \sum_{a=1}^K w_a f_a$,

$$\begin{aligned} \sup_{g \in \mathcal{F}(f_0)} \varphi(f_0, g, \rho) &= \rho^{\frac{1}{d}} \Delta_d \sup_{\lambda_1, \lambda_2, \dots, \lambda_K} \sum_{a=1}^K \lambda_a \int \frac{f_a(y)}{\left(\sum_{b=1}^K w_b f_b(y)\right)^{\frac{1}{d}}} dy \\ &= \rho^{\frac{1}{d}} \Delta_d \max_{1 \leq a \leq K} \left\{ \int \frac{\lambda_a f_a(y)}{\left(\sum_{b=1}^K w_b f_b(y)\right)^{\frac{1}{d}}} dy \right\}, \end{aligned} \quad (13)$$

where the last step uses the fact that $\lambda_a \in [0, 1]$, for $1 \leq a \leq K$, and $\sum_{a=1}^K \lambda_a = 1$. Note that the RHS above is unknown, because the densities f_1, \dots, f_K , the weights w_1, \dots, w_K , as well as the number K of mixture components, are all unknown. However, if we can consistently estimate the RHS of (13), then the test which rejects H_0 in (3) when $T_{m,n}$ is greater than the estimated value of (13), would have zero asymptotic Type I error and would be powerful whenever g has some separation from the set $\mathcal{F}(f_0)$ (recall definition in (2)).

The approach described above is, in general, infeasible because nonparametric estimation of mixture parameters in multivariate problems, especially when the number K is unknown, can often be difficult. In the following, we show how in location families, one can obtain a slightly weaker upper bound on $\varphi(f_0, g, \rho)$, which is free of the unknown parameters, that can be used to construct a valid and powerful test for the remodeling hypothesis (3). To this end, consider $\{p(y|\theta) = p(y - \theta) : \theta \in \Theta\}$ a family of densities indexed by the parameter space $\Theta \subseteq \mathbb{R}^d$, where $p : \mathbb{R}^d \rightarrow \mathbb{R}_{\geq 0}$ such that $\int_{\mathbb{R}^d} p(y) dy = 1$. Throughout we assume that the densities in the family satisfy Assumption 1. Suppose the baseline samples U_1, U_2, \dots, U_m are i.i.d. from the density $f_0(\cdot) = \sum_{a=1}^K w_a p(\cdot|\theta_a)$, where $\theta_1, \dots, \theta_K \in \Theta$ are fixed (but unknown), and there exists a known constant $L > 0$ such that $w_a \geq L$, for all $1 \leq a \leq K$. If the infected samples V_1, V_2, \dots, V_n are i.i.d. from a density g in \mathbb{R}^d , then the hypothesis of remodeling (2), in this parametric setting, becomes,

$$H_0 : g \in \mathcal{F}(\boldsymbol{\theta}) \quad \text{versus} \quad H_A : g \notin \mathcal{F}(\boldsymbol{\theta}), \quad (14)$$

where $\boldsymbol{\theta} = (\theta_1, \dots, \theta_K)$ and $\mathcal{F}(\boldsymbol{\theta})$ is defined as follows:

$$\mathcal{F}(\boldsymbol{\theta}) = \left\{ q(\cdot) = \sum_{a=1}^K \lambda_a p(\cdot|\theta_a) : \lambda_a \in [0, 1], \text{ for } 1 \leq a \leq K, \text{ and } \sum_{a=1}^K \lambda_a = 1 \right\},$$

is the collection of K -mixtures of $p(\cdot|\theta_1), p(\cdot|\theta_2), \dots, p(\cdot|\theta_K)$. Note that under the null H_0 , $g(\cdot) = \sum_{a=1}^K \lambda_a p(\cdot|\theta_a)$, for some $\lambda_1, \lambda_2, \dots, \lambda_K \in [0, 1]$, such that $\sum_{a=1}^K \lambda_a = 1$. Then using $\sum_{a=1}^K w_a p(y|\theta_a) > w_b p(y|\theta_b) \geq L p(y|\theta_b)$, for all $b \in \{1, 2, \dots, K\}$,

$$\begin{aligned} \varphi(f_0, g, \rho) &= \rho^{\frac{1}{d}} \Delta_d \sum_{a=1}^K \lambda_a \int \frac{p(y|\theta_a)}{\left(\sum_{b=1}^K w_b p(y|\theta_b)\right)^{\frac{1}{d}}} dy \\ &= \frac{\rho^{\frac{1}{d}} \Delta_d}{L^{\frac{1}{d}}} \int p(z)^{1-\frac{1}{d}} dz = \gamma, \end{aligned} \quad (15)$$

where the last step follows by the change of variable $z = y - \theta_a$. Note that the constant γ depends on L (the lower bound on the mixing weights of the baseline population), the dimension d , and the base

function p defining the location family (which is assumed to be known); but not on the unknown means $(\theta_1, \theta_2, \dots, \theta_K)$, the unknown weights (w_1, w_2, \dots, w_K) , or the number of components, and hence can be directly calculated. This implies that the test which rejects when $T_{m,n} > \gamma$, would have zero asymptotic Type I error, and would also be powerful whenever g has some separation from the set of possible null distributions $\mathcal{F}(f_0)$, as explained below.

The corollary below shows how the bound in (15) can be used to construct a test based on $T_{m,n}$ which is powerful for mixtures of radially symmetric distributions, such as Gaussian mixtures and t -mixtures, among others. Hereafter, we assume $p(y) = r(\|y\|)$ is radially symmetric, where $r : \mathbb{R}_{\geq 0} \rightarrow \mathbb{R}_{\geq 0}$ is a uniformly continuous function, such that $\int_{\mathbb{R}^d} r(\|y\|) dy = 1$. (Recall, $\|y\|$ denotes the Euclidean norm of $y \in \mathbb{R}^d$.)

Corollary 1. *For the testing problem (14) in the family $\{p(y|\theta) = r(\|y - \theta\|) : \theta \in \Theta\}$, the following hold:*

- For any $g \in \mathcal{F}(\theta)$, with γ as defined in (15), we have

$$\lim_{m,n \rightarrow \infty} \mathbb{P}_{f_0,g}(T_{m,n} > \gamma) = 0. \quad (16)$$

- There exists $\varepsilon(\gamma) > 0$ such that

$$\lim_{m,n \rightarrow \infty} \mathbb{P}_{f_0,g}(T_{m,n} > \gamma) = 1, \quad (17)$$

for any $g(y) = \sum_{a=1}^K \bar{\lambda}_a p(y|\theta'_a)$ with $\min_{1 \leq a, b \leq K} \|\theta'_a - \theta_b\| \mathbf{1}\{\bar{\lambda}_a > 0\} \geq \varepsilon(\gamma)$.

The proof of the corollary is given in the supplementary materials (Section C). Note that the condition on $g(y)$ in (17) quantifies a natural notion of separation between g and the set $\mathcal{F}(\theta)$, by assuming that at least one of the mixture means of g is ε -far (in L_2 -distance) from all the unknown null means of the baseline density. Explicit bounds on the separation $\varepsilon(\gamma)$ can be obtained from the proof of Corollary 1, based on the tail decay of the base density p (details given in supplementary materials, Section C).

6 Discussion

We propose a novel nearest neighbor based two-sample test for detecting changes between the baseline and the case samples, in the presence of heterogeneity, as is often the case in single-cell virology. For integrative analysis involving datasets collected from different experiments with varying external conditions, batch-effect corrections are needed before applying our methodology. Our testing procedure is

specially designed for mass cytometry based techniques (Bendall et al., 2011, Giesen et al., 2014) which produces moderate dimensional ($d \sim 50$) cellular characteristics. In the future, it will be interesting to extend our methodology for dealing with single-cell RNA-seq based techniques (Huang et al., 2018, Hwang et al., 2018, Jaitin et al., 2014, Schiffman et al., 2017), which can produce highly multivariate phenotypes ($d \sim 10^4$). A possible approach can be based on random projections of the d dimensional cellular characteristics to a lower dimensional space and then using our testing procedure on the reduced data. Also, it will be interesting to develop efficient testing procedures where the underlying population contains heterogeneous subpopulations with highly varying sizes including some very rare subpopulations. Finally, extending our hypothesis testing framework to distinguish between depletion and enrichment in remodeled cells will be important.

Acknowledgements

We are grateful to Ann Arvin, Nadia Roan, Adrish Sen, Nandini Sen and Nancy Zhang for numerous stimulating discussions. We thank the Editor, the Associate Editor and three referees for constructive suggestions that greatly improved the paper.

A Proof of Proposition 1

Recall that for U_1, \dots, U_m are i.i.d. f_0 and V_1, \dots, V_n are i.i.d. g . Then, in the usual asymptotic regime, by Theorem 2 of Henze and Penrose (1999), almost surely,

$$\frac{\mathcal{R}(\mathbf{U}_m, \mathbf{V}_n)}{m+n} \xrightarrow{a.s.} 1 - \delta(f_0, g, \rho) \quad (18)$$

where $\delta(f_0, g, \rho) = \int \frac{f^2(x) + \rho^2 g^2(x)}{(1+\rho)(f_0(x) + \rho g(x))} dx$.

Now, by Remark 1 of Henze and Penrose (1999) for any fixed $g \in \mathcal{F}(f_0) \setminus \{f_0\}$,

$$1 - \delta(f_0, g, \rho) < 1 - \delta(f_0, f_0, \rho) = \frac{2\rho}{(1+\rho)^2}.$$

Note that for any fixed $\alpha \in (0, 1/2)$, $\frac{C_{m,n}(\alpha)}{m+n} \rightarrow \frac{2\rho}{(1+\rho)^2}$ almost surely. Therefore, by (18), for any fixed $g \in \mathcal{F}(f_0) \setminus \{f_0\}$, $\mathcal{R}(\mathbf{U}_m, \mathbf{V}_n) < C_{m,n}(\alpha)$ almost surely, and the result follows.

B Proof of Theorem 1

The proof of Theorem 1 is an immediate consequence of the following two lemmas. The first lemma computes the limit of $n^{\frac{1}{d}} \bar{D}_{m,n}$.

Lemma 1. *Let D_1, D_2, \dots, D_n be as defined in equation (2.5). Then, under Assumption 1, as $m, n \rightarrow \infty$,*

$$\frac{1}{n^{1-\frac{1}{d}}} \sum_{i=1}^n D_i \xrightarrow{L_2} \rho^{\frac{1}{d}} \zeta_1 \int \frac{g(y)}{f_0(y)^{\frac{1}{d}}} dy, \quad (19)$$

where ζ_1 is as defined in the statement of Theorem 1.

The next lemma computes the limit of $n^{\frac{1}{d}} \bar{C}_{m,n}$, which combined with Lemma 1 completes the proof of Theorem 1.

Lemma 2. *Let C_1, C_2, \dots, C_n be as defined in equation (2.6). Then, under Assumption 1, as $m, n \rightarrow \infty$,*

$$\frac{1}{n^{1-\frac{1}{d}}} \sum_{i=1}^n C_i \xrightarrow{L_2} \rho^{\frac{1}{d}} \zeta_2 \int \frac{g(y)}{f_0(y)^{\frac{1}{d}}} dy, \quad (20)$$

where ζ_2 is as defined in the statement of Theorem 1.

The proofs of Lemma 1 and Lemma 2 are given below in Section B.2 and Section B.3, respectively. We begin with some preliminaries about Poisson processes and stabilization of geometric functionals, introduced by Penrose and Yukich (2003), in Section B.1 below.

B.1 Preliminaries

Given $z \in \mathbb{R}^d$, denote by $\varphi(z, \mathcal{Z})$ a measurable \mathbb{R}^+ valued function defined for all locally finite set $\mathcal{Z} \subset \mathbb{R}^d$ and $z \in \mathcal{Z}$. If $z \notin \mathcal{Z}$, then $\varphi(z, \mathcal{Z}) := \varphi(z, \mathcal{Z} \cup \{z\})$. The function φ is said to be *translation invariant* if $\varphi(y + z, y + \mathcal{Z}) = \varphi(z, \mathcal{Z})$. Penrose and Yukich (2003) defined stabilizing functions as follows:

Definition 1. (Penrose and Yukich (2003)) For any locally finite point set $\mathcal{Z} \subset \mathbb{R}^d$ and any integer $M \in \mathbb{N}$,

$$\bar{\varphi}(\mathcal{Z}, M) := \sup_{N \in \mathbb{N}} \left(\operatorname{esssup}_{\substack{\mathcal{A} \subset \mathbb{R}^d \setminus B(0, M) \\ |\mathcal{A}| = N}} \{ \varphi(0, \mathcal{Z} \cap B(0, M) \cup \mathcal{A}) \} \right)$$

and

$$\underline{\varphi}(\mathcal{Z}, M) := \inf_{N \in \mathbb{N}} \left(\operatorname{essinf}_{\substack{\mathcal{A} \subset \mathbb{R}^d \setminus B(0, M) \\ |\mathcal{A}| = N}} \{ \varphi(0, \mathcal{Z} \cap B(0, M) \cup \mathcal{A}) \} \right),$$

where the essential supremum/infimum is taken with respect to the Lebesgue measure on \mathbb{R}^{dN} . The functional φ is said to *stabilize* \mathcal{Z} if

$$\liminf_{M \rightarrow \infty} \varphi(\mathcal{Z}, M) = \overline{\lim}_{M \rightarrow \infty} \varphi(\mathcal{Z}, M) = \varphi(0, \mathcal{Z}). \quad (21)$$

We will be interested in functionals that stabilize almost surely on \mathcal{P}_λ , the homogeneous Poisson process with rate λ in \mathbb{R}^d . Note that with probability 1, $\overline{\varphi}(\mathcal{P}_\lambda, M)$ is nonincreasing in M and $\underline{\varphi}(\mathcal{P}_\lambda, M)$ is nondecreasing in M , therefore, they both converge. The definition of stabilization in (21) means they converge to the same limit almost surely. Note that any functional $\varphi(z, \mathcal{Z})$ which depends only on the points of \mathcal{Z} within a fixed distance of z is stabilizing on \mathcal{P}_λ . In our proofs, we will consider the following two functionals:

- For $y \in \mathbb{R}^d$, and $\mathcal{Z} \subset \mathbb{R}^d$ finite, define

$$\zeta_1(y, \mathcal{Z}) := \sum_{z \in \mathcal{Z}} \|y - z\| \mathbf{1}\{z = N(y, \mathcal{Z})\}, \quad (22)$$

which is the distance from y to its nearest neighbor in \mathcal{Z} .

- For $y \in \mathbb{R}^d$, and $\mathcal{Z} \subset \mathbb{R}^d$ finite, define

$$\zeta_2(y, \mathcal{Z}) := \sum_{z_1 \in \mathcal{Z}} \sum_{z_2 \in \mathcal{Z} \setminus \{z_1\}} \|z_1 - z_2\| \mathbf{1}\{z_1 = N(y, \mathcal{Z}) \text{ and } z_2 = N(z_1, \mathcal{Z} \setminus \{y\})\}, \quad (23)$$

which is the distance between the nearest neighbor of y in \mathcal{Z} and its nearest neighbor in \mathcal{Z} .

It is easy to verify that both the functionals $\zeta_1(\cdot, \cdot)$ and $\zeta_2(\cdot, \cdot)$ stabilize \mathcal{P}_λ , for all $\lambda > 0$. This is because the set of edges incident to the origin in the directed 1-nearest neighbor (NN) graph⁴ is unaffected by the addition or removal of points outside a ball of almost surely finite radius (Penrose and Yukich, 2003, Theorem 2.4).

B.2 Proof of Lemma 1

We now proceed to prove Lemma 1. We begin by noting that $\mathbb{E}(\overline{D}_{m,n}) = \mathbb{E}(D_1)$ and

$$\mathbb{E}(D_1) = \sum_{j=1}^m \mathbb{E}\|V_1 - U_j\| \mathbf{1}\{U_j = N(V_1, \mathbf{U}_m)\} = \mathbb{E}\zeta_1(V_1, \mathbf{U}_m), \quad (24)$$

⁴Given a finite set $S \subset \mathbb{R}^d$, the directed 1-nearest neighbor graph (1-NN) is a graph with vertex set S with a directed edge (a, b) , for $a, b \in S$, if b is the nearest neighbor of a in S .

where $\zeta_1(\cdot, \cdot)$ is as defined above in (22) and $\mathbf{U}_m = \{U_1, U_2, \dots, U_m\}$ are i.i.d. points from the density f_0 . Note that, by translation invariance,

$$\begin{aligned}\zeta_1(\mathbf{0}, m^{\frac{1}{d}}(\mathbf{U}_m - V_1)) &:= m^{\frac{1}{d}} \sum_{j=1}^m \|V_1 - U_j\| \mathbf{1}\{m^{\frac{1}{d}}(U_j - V_1) = N(\mathbf{0}, m^{\frac{1}{d}}(\mathbf{U}_m - V_1))\} \\ &= m^{\frac{1}{d}} \sum_{j=1}^m \|V_1 - U_j\| \mathbf{1}\{U_j = N(V_1, \mathbf{U}_m)\} \\ &= m^{\frac{1}{d}} \zeta_1(V_1, \mathbf{U}_m).\end{aligned}\tag{25}$$

The following lemma shows that the second moment of $\zeta_1(\mathbf{0}, m^{\frac{1}{d}}(\mathbf{U}_m - V_1))$ is bounded, under Assumption 1.

Lemma 3. *For densities f_0 and g as in Assumption 1,*

$$\sup_{m \in \mathbb{N}} \mathbb{E} \zeta_1(\mathbf{0}, m^{\frac{1}{d}}(\mathbf{U}_m - V_1))^2 \lesssim_d 1.$$

Proof. Note for $d \leq 2$, the result holds trivially, by the boundedness of the support. Hence, assuming, $d \geq 3$, and taking squares in (25) gives,

$$\begin{aligned}\zeta_1(\mathbf{0}, m^{\frac{1}{d}}(\mathbf{U}_m - V_1))^2 &:= m^{\frac{2}{d}} \sum_{1 \leq j_1, j_2 \leq m} \|V_1 - U_{j_1}\| \cdot \|V_1 - U_{j_2}\| \mathbf{1}\{U_{j_1} = N(V_1, \mathbf{U}_m), U_{j_2} = N(V_1, \mathbf{U}_m)\} \\ &\lesssim m^{\frac{2}{d}} \sum_{j=1}^m \|V_1 - U_j\|^2 \mathbf{1}\{U_j = N(V_1, \mathbf{U}_m)\},\end{aligned}\tag{26}$$

using the inequality $ab \leq \frac{a^2+b^2}{2}$ and the fact $\sum_{j=1}^m \mathbf{1}\{U_j = N(V_1, \mathbf{U}_m)\} = 1$. Now, for n large enough,

$$\begin{aligned}m^{\frac{2}{d}} \mathbb{E} \sum_{j=1}^m \|V_1 - U_j\|^2 \mathbf{1}\{U_j = N(V_1, \mathbf{U}_m)\} &= \frac{m^{\frac{2}{d}}}{n} \mathbb{E} \sum_{i=1}^n \sum_{j=1}^m \|V_i - U_j\|^2 \mathbf{1}\{U_j = N(V_i, \mathbf{U}_m)\} \\ &\lesssim_d \frac{1}{n^{1-\frac{2}{d}}} \mathbb{E} \phi(\mathbf{V}_n, \mathbf{U}_n),\end{aligned}\tag{27}$$

where the functional $\phi(A, B) := \sum_{a \in A} \sum_{b \in B} \|a - b\|^2 \mathbf{1}\{b = N(a, B)\}$, where $A, B \subset \mathbb{R}^d$ are finite and disjoint. Note that for any partition $\{S_0, S_1, \dots\}$ of \mathbb{R}^d ,

$$\phi(A, B) \leq \sum_{K=0}^{\infty} \phi(A \cap S_K, B \cap S_K),\tag{28}$$

that is, the functional ϕ is subadditive. (Note that the sum above is, in fact, finite because the sets A and

B are finite.) Then by a modification of (Yukich, 2006, Lemma 3.3), one can obtain the growth bound $\phi(A, B) \leq \text{diam}(A \cup B)^2 |A \cup B|^{\frac{d-2}{d}}$. Now, choosing S_0 to be the ball of radius 2 centered at the origin, and S_K to be the annulus centered at the origin with inner radius 2^K and outer radius 2^{K+1} , for $K \geq 1$, it follows from (28) that

$$\phi(\mathbf{V}_n, \mathbf{U}_m) \leq \sum_{K=0}^{\infty} 2^{2K} \left| \sum_{i=1}^n \mathbf{1}\{V_i \in S_K\} + \sum_{j=1}^m \mathbf{1}\{U_j \in S_K\} \right|^{\frac{d-2}{d}}.$$

Now, taking expectations above and the Jensen's inequality gives, for n large enough,

$$\frac{1}{n^{1-\frac{2}{d}}} \mathbb{E}\phi(\mathbf{V}_n, \mathbf{U}_m) \lesssim_d \sum_{K=0}^{\infty} 2^{2K} \mathbb{P}(V_1 \in S_K)^{\frac{d-2}{d}} + \sum_{K=0}^{\infty} 2^{2K} \mathbb{P}(U_1 \in S_K)^{\frac{d-2}{d}},$$

both of which are finite by the integrality assumptions on f_0 and g (using arguments in (Yukich, 2006, Page 85)). The result now follows by combining the bound above with (26) and (27). \square

The lemma above shows that the sequence $\{\zeta_1(\mathbf{0}, m^{\frac{1}{d}}(\mathbf{U}_m - V_1))\}_{M \geq 1}$ is uniformly integrable. Now, since the functional $\zeta_1(\cdot, \cdot)$ stabilizes on homogeneous Poisson processes, by arguments similar to the proof of (Yukich, 2013, Lemma 8.1), it follows that

$$\lim_{M \rightarrow \infty} \mathbb{E}\zeta_1(\mathbf{0}, m^{\frac{1}{d}}(\mathbf{U}_m - V_1)) = \mathbb{E}\zeta_1(\mathbf{0}, \mathcal{P}_{f_0(V)}), \quad (29)$$

where $\zeta_1(\mathbf{0}, \mathcal{P}_1)$ is as defined in equation (5.2), V is a random variable distributed according to the density g , and $\mathcal{P}_{f_0(V)}$ is a Cox process with intensity measure $f_0(V)$, which is a Poisson process with a random intensity measure $f_0(V)$. Conditioning on V gives,

$$\mathbb{E}\zeta_1(\mathbf{0}, \mathcal{P}_{f_0(V)}) = \int \mathbb{E}\zeta_1(\mathbf{0}, \mathcal{P}_{f_0(y)}) g(y) dy = \mathbb{E}\zeta_1(\mathbf{0}, \mathcal{P}_1) \int \frac{g(y)}{f_0(y)^{\frac{1}{d}}} dy,$$

where the last step uses $\mathcal{P}_\lambda \stackrel{D}{=} \lambda^{-\frac{1}{d}} \mathcal{P}_1$, for any $\lambda > 0$. This implies, by (24), (25), and (29), that

$$m^{\frac{1}{d}} \mathbb{E}(\bar{D}_{m,n}) = \mathbb{E}\zeta_1(\mathbf{0}, m^{\frac{1}{d}}(\mathbf{U}_m - V_1)) \rightarrow \mathbb{E}(\zeta_1(\mathbf{0}, \mathcal{P}_1)) \int \frac{g(y)}{f_0(y)^{\frac{1}{d}}} dy.$$

Then, recalling $n/m \rightarrow \rho$ gives,

$$\mathbb{E} \left(\frac{1}{n^{1-\frac{1}{d}}} \sum_{i=1}^n D_i \right) \rightarrow \rho^{\frac{1}{d}} \mathbb{E}(\zeta_1(\mathbf{0}, \mathcal{P}_1)) \int \frac{g(y)}{f_0(y)^{\frac{1}{d}}} dy, \quad (30)$$

which establishes the limit in (19) in expectation.

To complete the proof of the lemma we need to show that the variance of the LHS in (19) goes to zero. To this end, note that

$$\mathbb{E} \left(\frac{1}{n^{1-\frac{1}{d}}} \sum_{i=1}^n D_i \right)^2 = \frac{1}{n^{1-\frac{2}{d}}} \mathbb{E} D_1^2 + \frac{n(n-1)}{n^2} n^{\frac{2}{d}} \mathbb{E} D_1 D_2 = (1 + o(1)) n^{\frac{2}{d}} \mathbb{E} D_1 D_2 + o(1), \quad (31)$$

since $n^{\frac{2}{d}} \mathbb{E} D_1^2 \lesssim_d 1$, by Lemma 3. Next, note that

$$\begin{aligned} m^{\frac{2}{d}} \mathbb{E}(D_1 D_2) &= m^{\frac{2}{d}} \sum_{j_1=1}^m \sum_{j_2=1}^m \mathbb{E} \|V_1 - U_{j_1}\| \|V_2 - U_{j_2}\| \mathbf{1}\{U_{j_1} = N(V_1, \mathbf{U}_m)\} \mathbf{1}\{U_{j_2} = N(V_2, \mathbf{U}_m)\} \\ &= m^{\frac{2}{d}} \sum_{j_1=1}^m \|V_1 - U_{j_1}\| \mathbf{1}\{U_{j_1} = N(V_1, \mathbf{U}_m)\} \sum_{j_2=1}^m \|V_2 - U_{j_2}\| \mathbf{1}\{U_{j_2} = N(V_2, \mathbf{U}_m)\} \\ &= \mathbb{E} \zeta_1(\mathbf{0}, m^{\frac{1}{d}}(\mathbf{U}_m - V_1)) \zeta_1(\mathbf{0}, m^{\frac{1}{d}}(\mathbf{U}_m - V_2)). \end{aligned}$$

Now, by arguments similar to the proof of (Yukich, 2013, Proposition 3.1), it follows that

$$\lim_{M \rightarrow \infty} m^{\frac{2}{d}} \mathbb{E}(D_1 D_2) = \lim_{M \rightarrow \infty} \mathbb{E} \zeta_1(\mathbf{0}, m^{\frac{1}{d}}(\mathbf{U}_m - V_1)) \zeta_1(\mathbf{0}, m^{\frac{1}{d}}(\mathbf{U}_m - V_2)) = \mathbb{E} \zeta_1(\mathbf{0}, \mathcal{P}_{f_0(V)})^2,$$

where, as before, V is a random variable distributed according to the density g , and $\mathcal{P}_{f_0(V)}$ is a Cox process with intensity measure $f_0(V)$. This combined with (31) and (30), shows that

$$\text{Var} \left(\frac{1}{n^{1-\frac{1}{d}}} \sum_{i=1}^n D_i \right) \rightarrow 0.$$

This completes the proof of Lemma 1. □

B.3 Proof of Lemma 2

Denote $[m] := \{1, 2, \dots, m\}$. To begin with note that $\mathbb{E}(\bar{C}_{m,n}) = \mathbb{E}(C_1)$ and

$$\begin{aligned} \mathbb{E}(C_1) &= \sum_{j \in [m]} \sum_{s \in [m] \setminus \{j\}} \mathbb{E} \|U_j - U_s\| \mathbf{1}\{U_s = N(V_1, \mathbf{U}_m) \text{ and } U_j = N(U_s, \mathbf{U}_m)\} \\ &= \zeta_2(V_1, \mathbf{U}_m). \end{aligned} \quad (32)$$

As in (25), by translation invariance,

$$\begin{aligned}\zeta_2(\mathbf{0}, m^{\frac{1}{d}}(\mathbf{U}_m - V_1)) &= m^{\frac{1}{d}} \sum_{j \in [m]} \sum_{s \in [m] \setminus \{j\}} \|U_j - U_s\| \mathbf{1}\{U_s = N(V_1, \mathbf{U}_m) \text{ and } U_j = N(U_s, \mathbf{U}_m)\} \\ &= m^{\frac{1}{d}} \zeta_2(V_1, \mathbf{U}_m).\end{aligned}\quad (33)$$

Now, as in Lemma 3, it can be shown that $\sup_{m \in \mathbb{N}} \mathbb{E} \zeta_2(\mathbf{0}, m^{\frac{1}{d}}(\mathbf{U}_m - V_1))^2 \lesssim_d 1$. Therefore, since the functional $\zeta_2(\cdot, \cdot)$ stabilizes on homogeneous Poisson processes, by arguments similar to the proof of (Yukich, 2013, Lemma 8.1), it follows that

$$\lim_{M \rightarrow \infty} \mathbb{E} \zeta_2(\mathbf{0}, m^{\frac{1}{d}}(\mathbf{U}_m - V_1)) = \mathbb{E} \zeta_2(\mathbf{0}, \mathcal{P}_{f_0(V)}) = f_0(y)^{-\frac{1}{d}} \mathbb{E} \zeta_2(\mathbf{0}, \mathcal{P}_1) \quad (34)$$

where $\zeta_2(\mathbf{0}, \mathcal{P}_1)$ is as defined in equation (5.2), V is a random variable distributed according to the density g , and $\mathcal{P}_{f_0(V)}$ is a Cox process with intensity measure $f_0(V)$. Then, recalling $n/m \rightarrow \rho$, and combining (32), (33), and (34) gives,

$$\mathbb{E} \left(\frac{1}{n^{1-\frac{1}{d}}} \sum_{i=1}^n C_i \right) \rightarrow \rho^{\frac{1}{d}} \mathbb{E} \zeta_2(\mathbf{0}, \mathcal{P}_1) \int \frac{g(y)}{f_0(y)^{\frac{1}{d}}} dy.$$

which establishes the limit in (20) in expectation.

Finally, similar to the proof of Lemma 1, it can be shown that the variance of the LHS in (20) goes to zero, completing the proof. \square

As mentioned earlier, there does not appear to be a closed form expression for $\zeta_2 := \mathbb{E} \zeta_2(\mathbf{0}, \mathcal{P}_1)$. However, by an application of the FKG inequality for Poisson processes (Janson, 1984, Last and Penrose, 2017), it can be shown that $\zeta_2 \geq \zeta_1$. This is described in the following remark.

Remark 1. *From the definition of ζ_2 , we get*

$$\zeta_2 := \mathbb{E}(\zeta_2(\mathbf{0}, \mathcal{P}_1)) = \int \int \|w' - b\| \mathbb{P}(b = N(0, \mathcal{P}_1^{0,b}) \text{ and } w' = N(b, \mathcal{P}_1^{0,b} \setminus \{0\})) db dw'. \quad (35)$$

For $b, w' \in \mathbb{R}^d$ fixed, consider the functions $\mathbf{1}\{b = N(0, \mathcal{P}_1^{0,b})\}$ and $\mathbf{1}\{w' = N(b, \mathcal{P}_1^{0,b} \setminus \{0\})\}$, defined on the Poisson point process \mathcal{P}_1^0 . Now, let Γ and Γ' be two realizations of the point process \mathcal{P}_1^0 . Note that by if $\Gamma \subset \Gamma'$, then $\mathbf{1}\{b = N(0, \Gamma')\} \leq \mathbf{1}\{b = N(0, \Gamma)\}$, because if b is a nearest neighbor of the origin in Γ' , it will be also be nearest neighbor of the origin in the smaller set Γ . Similarly, for $\Gamma \subset \Gamma'$, $\mathbf{1}\{w' = N(b, \Gamma' \setminus \{0\})\} \leq \mathbf{1}\{w' = N(b, \Gamma \setminus \{0\})\}$. Therefore, both the functions $\mathbf{1}\{b = N(0, \mathcal{P}_1^{0,b})\}$ and

$\mathbf{1}\{w' = N(b, \mathcal{P}_1^{0,b} \setminus \{0\})\}$ are nonincreasing, and by an application of the FKG inequality for functions on Poisson processes (Janson, 1984, Lemma 2.1), it follows that

$$\mathbb{P}(b = N(0, \mathcal{P}_1^{0,b}) \text{ and } w' = N(b, \mathcal{P}_1^{0,b} \setminus \{0\})) \geq \mathbb{P}(b = N(0, \mathcal{P}_1^0))\mathbb{P}(w' = N(b, \mathcal{P}_1^b))$$

This combined with (35) gives,

$$\begin{aligned} \zeta_2 &\geq \int \int \|w' - b\| \mathbb{P}(b = N(0, \mathcal{P}_1^0)) \mathbb{P}(w' = N(b, \mathcal{P}_1^b)) db dw' \\ &= \int \int \|w' - b\| e^{-V_d \|b\|} e^{-V_d \|w' - b\|} db dw' \\ &= \left(\int e^{-V_d \|b\|} db \right) \left(\int \|v\| e^{-V_d \|v\|} dv \right) = \zeta_1, \end{aligned}$$

where the last step uses the definition of ζ_1 from equation (5.4), and $\int e^{-V_d \|b\|} db = S_d \int_0^\infty r^{d-1} e^{-V_d r^d} dr = V_d \int_0^\infty e^{-V_d y} dy = 1$.

d	ζ_1	ζ_2	$\Delta_d = \zeta_2 - \zeta_1$
1	0.5006	0.7493	0.2487
2	0.5008	0.5969	0.0961
3	0.5580	0.6155	0.0574
4	0.6187	0.6572	0.0385
5	0.6782	0.7054	0.0271
6	0.7361	0.7548	0.0187

Table 12: Numerical estimates of ζ_1 and ζ_2 .

Numerical estimates of the constants ζ_1 and ζ_2 for small dimensions are given in Table 12. This is computed using the average (over 20 iterations) of the values of $n^{\frac{1}{d}} \bar{D}_{m,n}$ and $n^{\frac{1}{d}} \bar{C}_{m,n}$ (recall equation (2.7)) with $m = n = 100000$ i.i.d uniform points in the d -dimensional unit cube $[0, 1]^d$.

C Proof of Corollary 1

Note that, by equation (5.7), for $g \in \mathcal{F}(\theta)$, $T_{m,n} \xrightarrow{P} \varphi(f_0, g, \rho) < \gamma$. This implies, $\lim_{m,n \rightarrow \infty} \mathbb{P}_{f_0, g}(T_{m,n} > \gamma) = 0$, which proves (5.8).

Under the alternative, suppose $g(y) = \sum_{a=1}^K \bar{\lambda}_a p(y|\theta'_a)$, such that, for some $1 \leq j \leq K$ with $\bar{\lambda}_j > 0$,

$\min_{1 \leq a \leq K} \|\theta'_j - \theta_a\| \geq \varepsilon(\gamma)$, where $\varepsilon(\gamma)$ will be chosen later. Then

$$\begin{aligned} \varphi(f_0, g, \rho) &= \rho^{\frac{1}{d}} \Delta_d \int \frac{g(y)}{f_0(y)^{\frac{1}{d}}} dy = \rho^{\frac{1}{d}} \Delta_d \sum_{a=1}^K \int \frac{\bar{\lambda}_a p(y|\theta'_a)}{\left(\sum_{b=1}^K w_b p(y|\theta_b)\right)^{\frac{1}{d}}} dy \\ &\geq \rho^{\frac{1}{d}} \Delta_d \int_{B(\theta'_j, 1)} \frac{\bar{\lambda}_j p(y|\theta'_j)}{\left(\sum_{b=1}^K w_b p(y|\theta_b)\right)^{\frac{1}{d}}} dy. \end{aligned} \quad (36)$$

Now, since the function $r(\cdot)$ is uniformly continuous and $\int_0^\infty r(z) dz < \infty$, it follows that $\lim_{z \rightarrow \infty} r(z) = 0$ (see discussion following (Niculescu and Popovici, 2011, Corollary 1)). This implies for every $M > 0$ there exists a $\eta(M, d) > 0$, such that $r(z) \leq M^{-\frac{1}{d}}$, for $z > \eta(M, d)$. Define

$$M := \frac{2\gamma}{\rho^{\frac{1}{d}} \Delta_d L \int_{B(0,1)} p(y) dy} \quad \text{and} \quad \varepsilon(\gamma) := \eta(M, d) + 1.$$

Take a point θ'_j such that $\|\theta'_j - \theta_a\| \geq \varepsilon(\gamma)$, for all $1 \leq a \leq K$. Then, for all $1 \leq a \leq K$, if $y \in B(\theta'_j, 1)$,

$$\eta(M, d) + 1 \leq \|\theta'_j - \theta_a\| \leq \|\theta'_j - y\| + \|y - \theta_a\| \leq 1 + \|y - \theta_a\|,$$

implies $\|y - \theta_a\| \geq \eta(M, d)$. Therefore, for all $1 \leq a \leq K$, if $y \in B(\theta'_j, 1)$, $p(y|\theta_a) = p(y - \theta_a) = r(\|y - \theta_a\|) \leq M^{-\frac{1}{d}}$ and $\sum_{a=1}^K w_a p(y|\theta_a) \leq M^{-\frac{1}{d}}$. Then, from (36),

$$\begin{aligned} \varphi(f_0, g, \rho) &\geq \rho^{\frac{1}{d}} \Delta_d \bar{\lambda}_j M \int_{B(\theta'_j, 1)} p(y|\theta'_j) dy = \rho^{\frac{1}{d}} \Delta_d \bar{\lambda}_j M \int_{B(\theta'_j, 1)} p(y - \theta'_j) dy \\ &\geq \rho^{\frac{1}{d}} \Delta_d L M \int_{B(0,1)} p(y) dy \\ &= 2\gamma. \end{aligned}$$

This implies $\lim_{m, n \rightarrow \infty} \mathbb{P}_{f_0, g}(T_{m, n} > \gamma) = 1$, since $T_{m, n} \xrightarrow{P} \varphi(f_0, g, \rho) > 2\gamma$, for g as above. This completes the proof of (5.9). \square

Note that the separation $\varepsilon(\gamma)$ depends on $\eta(M, d)$, the rate of decay of the tail of the base density p . For instance, when p is the standard multivariate normal distribution $N(0, I_d)$, then it suffices to choose $\eta(M, d) = K(d) \sqrt{\log M}$, where $K(d)$ is a constant depending on d .

D Additional Numerical Experiments

D.1 Sensitivity of the Numerical Experiments in Section 3 to the choice of τ_{fc}

We consider the setting of Experiment 2 in section 3.2 and report the sensitivity of our inference using TRUH to changes in the fold change constant τ_{fc} . Recall that in Experiment 2,

$$F_0 = 0.5 \text{Gam}_d(\text{shape} = 5\mathbf{1}_d, \text{rate} = \mathbf{1}_d, \Sigma_1) + 0.5 \text{Exp}_d(\text{rate} = \mathbf{1}_d, \Sigma_2),$$

where Gam_d and Exp_d are d dimensional Gamma and Exponential distributions. For generating correlated Gamma and Exponential variables, we use the Gaussian copula approach based function from the R-package `lcmix` (Dvorkin, 2012, Xue-Kun Song, 2000). We consider tapering matrices with positive and negative autocorrelations: $(\Sigma_1)_{ij} = 0.7^{|i-j|}$ and $(\Sigma_2)_{ij} = -0.9^{|i-j|}$ for $1 \leq i, j \leq d$. For simulating V_n from G , we consider the following two scenarios:

- Scenario I: Here, $G = \text{Exp}_d(\text{rate} = \mathbf{1}_d, \Sigma_2)$. In this case, G arises from only one of the components of F_0 , that is, $G \in \mathcal{F}(F_0)$.
- Scenario II: Here, $G = 0.1 \text{Gam}_d(\text{shape} = 10\mathbf{1}_d, \text{rate} = 0.5\mathbf{1}_d, \Sigma_1) + 0.9 \text{Exp}_d(\text{rate} = \mathbf{1}_d, \Sigma_2)$. In this setting, $G \notin \mathcal{F}(F_0)$ and the composite null H_0 is not true. When the ratio n/m is small, this scenario presents a difficult setting for detecting departures from H_0 as majority of the case samples from V_n will arise from $\text{Exp}_d(\text{rate} = \mathbf{1}_d, \Sigma_2)$ and the tests will rely on only a small fraction of samples from $\text{Gam}_d(\text{shape} = 10\mathbf{1}_d, \text{rate} = 0.5\mathbf{1}_d, \Sigma_1)$ to reject the null hypothesis.

Table 13: Rejection rates of TRUH at 5% level of significance: Experiment 2 and Scenario I wherein $H_0 : G \in \mathcal{F}(F_0)$ is true.

	$m = 500, n = 50$			$m = 2000, n = 200$		
τ_{fc}	$d = 5$	$d = 15$	$d = 30$	$d = 5$	$d = 15$	$d = 30$
1.0	0.000	0.000	0.000	0.000	0.000	0.000
1.2	0.000	0.000	0.000	0.000	0.000	0.000
1.4	0.000	0.000	0.000	0.000	0.000	0.000

Table 14: Rejection rates of TRUH at 5% level of significance: Experiment 2 and Scenario II wherein $H_0 : G \in \mathcal{F}(F_0)$ is false.

	$m = 500, n = 10$			$m = 2000, n = 40$		
τ_{fc}	$d = 5$	$d = 15$	$d = 30$	$d = 5$	$d = 15$	$d = 30$
1.0	0.580	0.580	0.580	0.880	0.940	0.960
1.2	0.500	0.560	0.580	0.820	0.860	0.900
1.4	0.460	0.480	0.500	0.780	0.760	0.700

Table 15: Rejection rates of TRUH at 5% level of significance under Dirichlet sampling of mixing proportions: Experiment 2 and Scenario I wherein $H_0 : G \in \mathcal{F}(F_0)$ is true.

τ_{fc}	$m = 500, n = 50$			$m = 2000, n = 200$		
	$d = 5$	$d = 15$	$d = 30$	$d = 5$	$d = 15$	$d = 30$
1.0	0.000	0.000	0.000	0.000	0.000	0.000
1.2	0.000	0.000	0.000	0.000	0.000	0.000
1.4	0.000	0.000	0.000	0.000	0.000	0.000

Tables 13 and 14 report the average rejection rates of TRUH across 100 repetitions of the test as τ_{fc} varies over $\{1, 1.2, 1.4\}$. We note that the rejection rates under Scenario II are bigger than those of Scenario I, which indicates that our proposed procedure is powerful against departures from the null hypothesis while the rejection rates under Scenario I are below the prespecified 0.05 level establishing that it is a conservative test across all the regimes considered in the table. These results also indicate that an appropriate choice of τ_{fc} must be bigger or equal to 1 for a value less than 1 may lead to incorrect rejections of the null hypothesis.

Table 16: Rejection rates of TRUH at 5% level of significance under Dirichlet sampling of mixing proportions: Experiment 2 and Scenario II wherein $H_0 : G \in \mathcal{F}(F_0)$ is false.

τ_{fc}	$m = 500, n = 10$			$m = 2000, n = 40$		
	$d = 5$	$d = 15$	$d = 30$	$d = 5$	$d = 15$	$d = 30$
1.0	0.580	0.580	0.580	0.880	0.940	0.960
1.2	0.500	0.560	0.580	0.840	0.860	0.900
1.4	0.440	0.480	0.500	0.780	0.760	0.700

The preceding analyses were based on sampling the mixing proportions $\{\lambda_1, \dots, \lambda_{\hat{K}}\}$ only from the corners of the \hat{K} dimensional simplex $\mathcal{S}_{\hat{K}}$ (see section 2.3). In what follows, we alter this sampling scheme and sample the \hat{K} mixing proportions from a Dirichlet distribution with parameters $\{\beta_1, \dots, \beta_{\hat{K}}\}$. We set $\beta_a = 0.1$ for $1 \leq a \leq \hat{K}$ and report the rejection rates under this sampling scheme in tables 15 and 16. With $\beta_a = 0.1$, the Dirichlet distribution places a large mass on the corners of the \hat{K} dimensional simplex which explains the similar trend in the rejections rates that is observed across both the scenarios in tables 15 and 16 when compared to tables 13 and 14, respectively.

D.2 Sensitivity of the Real Data Analysis in Section 4 to the choice of τ_{fc}

In section 4 the fold change constant τ_{fc} was set to 1.1. In this section we report the sensitivity of the results reported in section 4 for $\tau_{fc} \in \{1, 1.1, 1.3, 1.7, 2\}$. In tables 17 to 20 we report the p-values of the TRUH test statistic for testing remodeling under HIV infection under the four cases as described in section 4. For Cases 1 and 3, which are known to exhibit remodeling, we note from tables 17 and 19 that for $\tau_{fc} > 1.1$, the TRUH test statistic fails to detect τ remodeling across all four donors. This is not

Table 17: p-values of TRUH in CASE 1: Uninfected versus Nef-rich HIV Infected for entire 35 markers.

	Donor 1	Donor 2	Donor 3	Donor 4
τ_{fc}	$m = 24,984, n = 245$	$m = 31,552, n = 521$	$m = 17,704, n = 211$	$m = 22,830, n = 660$
1.0	< 0.001	< 0.001	< 0.001	< 0.001
1.1	< 0.001	< 0.001	< 0.001	< 0.001
1.3	0.082	0.05	0.086	0.292
1.7	1	1	1	1
2.0	1	1	1	1

Table 18: p-values of TRUH in CASE 2: Uninfected versus Nef-rich HIV Infected for 31 invariant markers.

	Donor 1	Donor 2	Donor 3	Donor 4
τ_{fc}	$m = 24,984, n = 245$	$m = 31,552, n = 521$	$m = 17,704, n = 211$	$m = 22,830, n = 660$
1.0	< 0.001	< 0.001	< 0.001	< 0.001
1.1	< 0.001	0.67	0.274	0.914
1.3	1	1	1	1
1.7	1	1	1	1
2.0	1	1	1	1

Table 19: p-values of TRUH in CASE 3: Uninfected versus Nef-deficient HIV Infected for the entire 35 markers.

	Donor 1	Donor 2	Donor 3	Donor 4
τ_{fc}	$m = 24,984, n = 129$	$m = 31,552, n = 382$	$m = 17,704, n = 174$	$m = 22,830, n = 440$
1.0	< 0.001	< 0.001	< 0.001	< 0.001
1.1	< 0.001	< 0.001	< 0.001	< 0.001
1.3	1	1	1	1
1.7	1	1	1	1
2.0	1	1	1	1

Table 20: p-values of TRUH in CASE 4: Uninfected versus Nef-deficient HIV Infected for the entire 31 invariant markers.

	Donor 1	Donor 2	Donor 3	Donor 4
τ_{fc}	$m = 24,984, n = 129$	$m = 31,552, n = 382$	$m = 17,704, n = 174$	$m = 22,830, n = 440$
1.0	< 0.001	< 0.001	< 0.001	< 0.001
1.1	0.58	0.94	0.464	0.524
1.3	1	1	1	1
1.7	1	1	1	1
2.0	1	1	1	1

unexpected since a relatively large value of τ_{fc} offers higher conservatism in rejecting the null hypothesis of no remodeling. Tables 18 and 20, on the other hand, represent cases of no remodeling and $\tau_{fc} \geq 1.1$ allows TRUH to correctly detect no remodeling for Cases 2 and 4.

D.3 Computation Time Comparisons

In this section we present a comparison of the computing time for each of the seven competing testing procedures under the settings of Scenarios I and II of Experiment 2 (see section 3.2) with $n = 15000$, $m = 150$ and $d \in \{5, 15, 30, 50\}$. Tables 21 and 22 report the average computing time in minutes across 10 repetitions of the testing problem as d varies. Here the computing time represents the time each test takes to generate a p-value. We note that the Energy test is extremely efficient with an average computation

Table 21: Mean computing time (in minutes) for the seven competing testing procedures under the setting of Scenario I Experiment 2. Here $n = 15000$, $m = 150$.

d	Energy	Crossmatch	E Count	GE Count	WE Count	MTE Count	TRUH
5	1.128	41.221	8.242	8.242	8.242	8.242	1.047
15	1.142	35.225	9.394	9.394	9.394	9.394	2.161
30	1.162	35.141	9.481	9.481	9.481	9.481	3.970
50	1.235	42.062	9.784	9.784	9.784	9.784	6.380

Table 22: Mean computing time (in minutes) for the seven competing testing procedures under the setting of Scenario II Experiment 2. Here $n = 15000$, $m = 150$.

d	Energy	Crossmatch	E Count	GE Count	WE Count	MTE Count	TRUH
5	1.107	45.604	7.277	7.277	7.277	7.277	1.003
15	1.147	37.688	7.502	7.502	7.502	7.502	2.099
30	1.117	32.858	7.581	7.581	7.581	7.581	3.634
50	1.150	46.575	6.833	6.833	6.833	6.833	6.044

time just over a minute for these scenarios. Our proposed testing procedure TRUH is the next best and is closely followed by the four variants of the Edge Count tests. The R package `gtests` that implements these variants of the Edge Count tests, spits the results for all these variants simultaneously and thus the different Edge Count tests exhibit the same performance in tables 21 and 22. We note that the computation time of TRUH increases with d , which is not surprising because the computational cost for running the 1-nearest neighbor algorithm is $O(nmd)$. The Edge Count tests, on the other hand, rely on a minimum spanning tree construction which has $O(n^2)$ complexity and dominates the overall running time. In our experiments, we find that the Crossmatch test is the slowest primarily because this test requires a number of computationally expensive steps such as ranking each of the d dimensions, computing and inverting the d dimensional covariance matrix of the ranks and finally calculating the $(n + m) \times (n + m)$ matrix of Mahalanobis distance between the rank pairs.

D.4 Influence of mixing proportions on the null distribution

To understand how the specific mixing proportions influence the null distribution of the TRUH statistic, we consider the setting of Experiment 2 (section 3.2 of the manuscript) where the uninfected cells arise from a 2-component mixture distribution given by $F_0 = 0.5 \text{Gam}_d(\text{shape} = 5\mathbf{1}_d, \text{rate} = \mathbf{1}_d, \Sigma_1) + 0.5 \text{Exp}_d(\text{rate} = \mathbf{1}_d, \Sigma_2)$. The infected cells arise from $G = \text{Exp}_d(\text{rate} = \mathbf{1}_d, \Sigma_2)$ for scenario I and from $G = 0.1\text{Gam}_d(\text{shape} = 10\mathbf{1}_d, \text{rate} = 0.5\mathbf{1}_d, \Sigma_1) + 0.9\text{Exp}_d(\text{rate} = \mathbf{1}_d, \Sigma_2)$ for scenario II. Thus scenario I represents preferential infection and scenario II represents remodeling. Here Gam_d and Exp_d are d dimensional Gamma and Exponential distributions.

Figure 10 plots the $\hat{K} = 2$ null distributions of the TRUH statistic under Scenario I. Here the bootstrap algorithm generates the mixing proportions $\{\lambda_1, \dots, \lambda_{\hat{K}}\}$ in step (i) only from the corners of the $\hat{K} = 2$

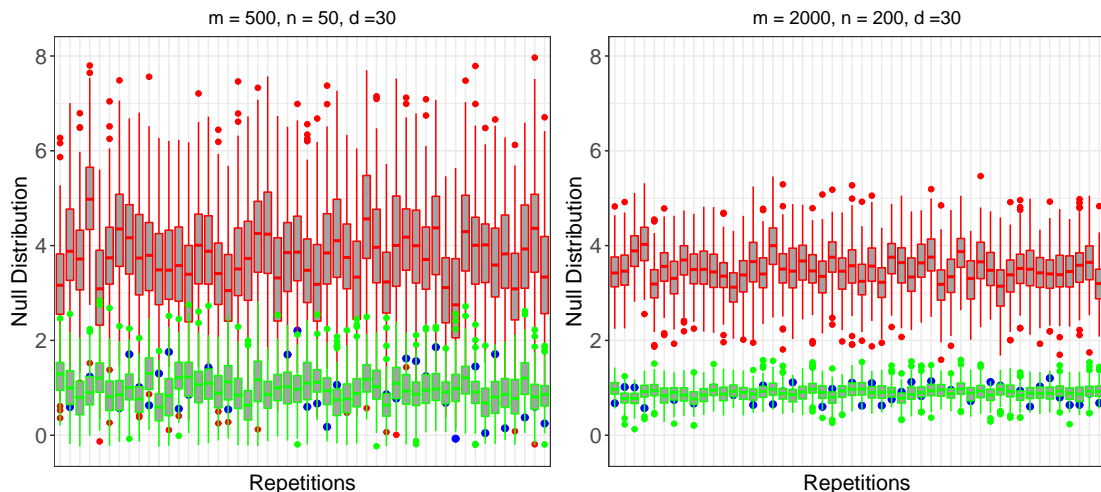


Figure 10: The red box plots and the green box plots represent $\hat{K} = 2$ null distributions for each of the 50 repetitions of Scenario I (H_0 is true) corresponding to mixing proportions $\{\lambda_1 = 1, \lambda_2 = 0\}$ and $\{\lambda_1 = 0, \lambda_2 = 1\}$ respectively. The blue dots are the TRUH test statistic in each repetition of the test. Left: Uninfected and Infected sample sizes are $m = 500, n = 50$ and dimensionality of each sample is $d = 30$. Right: $m = 2000, n = 200, d = 30$.

dimensional simplex $\mathcal{S}_{\hat{K}}$ and so there are $B_1 = \hat{K}$ such null distributions for each of the 50 repetitions of the test. The null distributions represented by the red box plots arise when the n pseudo infected cells are randomly sampled from the first component of F_0 , which corresponds to a configuration of mixing proportions given by $\{\lambda_1 = 1, \lambda_2 = 0\}$. The box plots in green, on the other hand, arise when the n pseudo infected cells are randomly sampled from the second component of F_0 , which corresponds to $\{\lambda_1 = 0, \lambda_2 = 1\}$. The blue dots represent the TRUH test statistic across the 50 repetitions of the test. Note that in Scenario I, the infected cells arise from the second component of F_0 and this explains why the TRUH test statistic, given by the blue dots, are closer to the box plots in green. However, the null distribution represented by the red box plots, which correspond to the mixing proportions $\{\lambda_1 = 1, \lambda_2 = 0\}$, offer more conservatism in rejecting the null hypothesis of no remodeling as far as Scenario I is concerned.

Figure 11, on the other hand, plots the $\hat{K} = 2$ null distributions of the TRUH statistic under Scenario II which is a case of remodeling. Here the TRUH test statistic is capped at 15 for ease of visual representation. Unlike Scenario I, the infected cells do not arise from the convex hull $\mathcal{F}(F_0)$ of F_0 , which explains why the TRUH test statistic are far away from the two null distributions. However, even in this scenario when the n pseudo infected cells are randomly sampled from the first component of F_0 , the corresponding null distribution (box plots in red) offers more conservatism in rejecting the null hypothesis of no remodeling than the null distribution that arises under the configuration $\{\lambda_1 = 0, \lambda_2 = 1\}$.

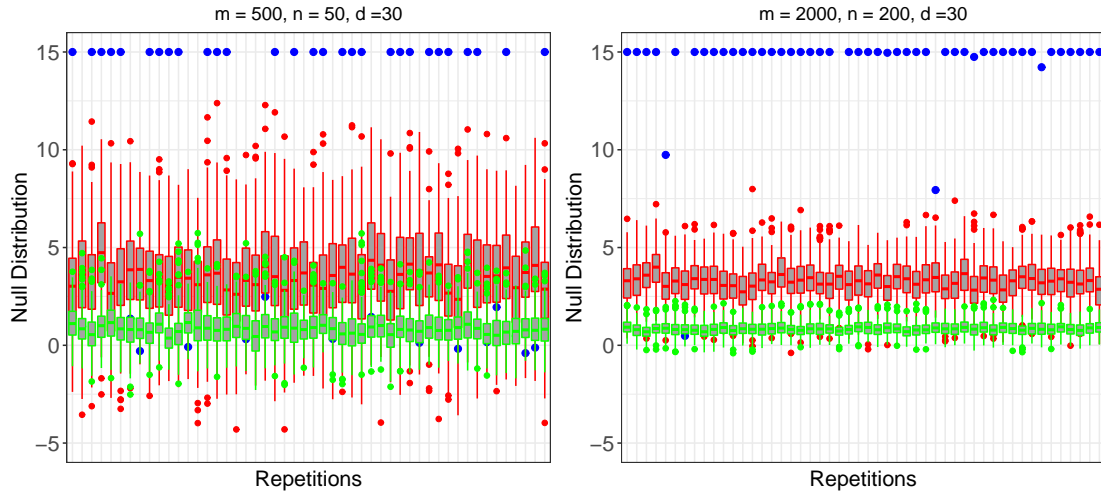


Figure 11: The red box plots and the green box plots represent $\hat{K} = 2$ null distributions for each of the 50 repetitions of Scenario II (H_0 is false) corresponding to mixing proportions $\{\lambda_1 = 1, \lambda_2 = 0\}$ and $\{\lambda_1 = 0, \lambda_2 = 1\}$ respectively. The blue dots are the TRUE test statistic in each repetition of the test and are capped at 15 for ease of visual representation. Left: Uninfected and Infected sample sizes are $m = 500, n = 50$ and dimensionality of each sample is $d = 30$. Right: $m = 2000, n = 200, d = 30$.

References

- Amir, E.-a. D., K. L. Davis, M. D. Tadmor, E. F. Simonds, J. H. Levine, S. C. Bendall, D. K. Shenfeld, S. Krishnaswamy, G. P. Nolan, and D. Pe'er (2013). visne enables visualization of high dimensional single-cell data and reveals phenotypic heterogeneity of leukemia. *Nature biotechnology* 31(6), 545–552.
- Aslan, B. and G. Zech (2005). New test for the multivariate two-sample problem based on the concept of minimum energy. *Journal of Statistical Computation and Simulation* 75(2), 109–119.
- Banerjee, T., B. B. Bhattacharya, and G. Mukherjee (2020). Supplement to a nearest-neighbor based nonparametric test for viral remodeling in heterogeneous single-cell proteomic data.
- Baringhaus, L. and C. Franz (2004). On a new multivariate two-sample test. *Journal of multivariate analysis* 88(1), 190–206.
- Basmaciogullari, S. and M. Pizzato (2014). The activity of nef on hiv-1 infectivity. *Frontiers in microbiology* 5, 232.
- Bendall, S. C., K. L. Davis, E.-a. D. Amir, M. D. Tadmor, E. F. Simonds, T. J. Chen, D. K. Shenfeld, G. P. Nolan, and D. Pe'er (2014). Single-cell trajectory detection uncovers progression and regulatory coordination in human b cell development. *Cell* 157(3), 714–725.

- Bendall, S. C., E. F. Simonds, P. Qiu, E.-a. I. . A. D. Amir, P. O. Krutzik, R. Finck, R. V. Bruggner, R. Melamed, A. Trejo, O. I. Ornatsky, R. S. Balderas, S. K. Plevritis, K. Sachs, D. Pe'er, S. D. Tanner, and G. P. Nolan (2011, May). Single-cell mass cytometry of differential immune and drug responses across a human hematopoietic continuum. *Science (New York, N.Y.)* 332(6030), 687–696.
- Berrett, T. B. and R. J. Samworth (2019a). Efficient two-sample functional estimation and the super-oracle phenomenon. *arXiv preprint arXiv:1904.09347*.
- Berrett, T. B. and R. J. Samworth (2019b). Nonparametric independence testing via mutual information. *Biometrika* 106(3), 547–566.
- Berrett, T. B., R. J. Samworth, and M. Yuan (2019). Efficient multivariate entropy estimation via k -nearest neighbour distances. *The Annals of Statistics* 47(1), 288–318.
- Bhattacharya, B. B. (2019). A general asymptotic framework for distribution-free graph-based two-sample tests. *Journal of the Royal Statistical Society: Series B (Statistical Methodology)* 81(3), 575–602.
- Bickel, P. J. (1969). A distribution free version of the smirnov two sample test in the p -variate case. *The Annals of Mathematical Statistics* 40(1), 1–23.
- Bruggner, R. V., B. Bodenmiller, D. L. Dill, R. J. Tibshirani, and G. P. Nolan (2014). Automated identification of stratifying signatures in cellular subpopulations. *Proceedings of the National Academy of Sciences* 111(26), E2770–E2777.
- Cannings, T. I., T. B. Berrett, and R. J. Samworth (2019). Local nearest neighbour classification with applications to semi-supervised learning. *arXiv preprint arXiv:1704.00642*.
- Cavrois, M., T. Banerjee, G. Mukherjee, N. Raman, R. Hussien, B. A. Rodriguez, J. Vasquez, M. H. Spitzer, N. H. Lazarus, J. J. Jones, et al. (2017). Mass cytometric analysis of hiv entry, replication, and remodeling in tissue cd4+ t cells. *Cell reports* 20(4), 984–998.
- Chaudhuri, R., O. W. Lindwasser, W. J. Smith, J. H. Hurley, and J. S. Bonifacino (2007). Downregulation of cd4 by human immunodeficiency virus type 1 nef is dependent on clathrin and involves direct interaction of nef with the ap2 clathrin adaptor. *Journal of virology* 81(8), 3877–3890.
- Chen, H., X. Chen, and Y. Su (2018). A weighted edge-count two-sample test for multivariate and object data. *Journal of the American Statistical Association* 113(523), 1146–1155.

- Chen, H. and J. H. Friedman (2017). A new graph-based two-sample test for multivariate and object data. *Journal of the American statistical association* 112(517), 397–409.
- Chen, L., W. W. Dou, and Z. Qiao (2013). Ensemble subsampling for imbalanced multivariate two-sample tests. *Journal of the American Statistical Association* 108(504), 1308–1323.
- Chung, J. H. and D. A. Fraser (1958). Randomization tests for a multivariate two-sample problem. *Journal of the American Statistical Association* 53(283), 729–735.
- Cover, T. and P. Hart (1967). Nearest neighbor pattern classification. *IEEE transactions on information theory* 13(1), 21–27.
- Cressie, N. (1976). On the logarithms of high-order spacings. *Biometrika* 63(2), 343–355.
- Deb, N. and B. Sen (2019). Multivariate rank-based distribution-free nonparametric testing using measure transportation. *arXiv preprint arXiv:1909.08733*.
- Devroye, L., L. Györfi, and G. Lugosi (2013). *A probabilistic theory of pattern recognition*, Volume 31. Springer Science & Business Media.
- Dvorkin, D. (2012). *lcmix: Layered and chained mixture models*. R package version 0.3/r5.
- Friedman, J. H. and L. C. Rafsky (1979). Multivariate generalizations of the wald-wolfowitz and smirnov two-sample tests. *The Annals of Statistics*, 697–717.
- Gadat, S., T. Klein, and C. Marteau (2016). Classification in general finite dimensional spaces with the k -nearest neighbor rule. *The Annals of Statistics* 44(3), 982–1009.
- Garcia, J. V. and A. D. Miller (1991). Serine phosphorylation-independent downregulation of cell-surface cd4 by nef. *Nature* 350(6318), 508.
- Ghosal, P. and B. Sen (2019). Multivariate ranks and quantiles using optimal transportation and applications to goodness-of-fit testing. *arXiv preprint arXiv:1905.05340*.
- Giesen, C., H. A. Wang, D. Schapiro, N. Zivanovic, A. Jacobs, B. Hattendorf, P. J. Schüffler, D. Grolmund, J. M. Buhmann, S. Brandt, et al. (2014). Highly multiplexed imaging of tumor tissues with subcellular resolution by mass cytometry. *Nature methods* 11(4), 417.
- Goria, M. N., N. N. Leonenko, V. V. Mergel, and P. L. Novi Inverardi (2005). A new class of random vector entropy estimators and its applications in testing statistical hypotheses. *Journal of Nonparametric Statistics* 17(3), 277–297.

- Gretton, A., K. M. Borgwardt, M. Rasch, B. Schölkopf, and A. J. Smola (2007). A kernel method for the two-sample-problem. In *Advances in neural information processing systems*, pp. 513–520.
- Hall, P. and N. Tajvidi (2002). Permutation tests for equality of distributions in high-dimensional settings. *Biometrika* 89(2), 359–374.
- Heckel, R. and H. Bölcskei (2015). Robust subspace clustering via thresholding. *IEEE Transactions on Information Theory* 61(11), 6320–6342.
- Henze, N. (1984). On the number of random points with nearest neighbour of the same type and a multivariate two-sample test. *Metrika* 31, 259–273.
- Henze, N. and M. Penrose (1999). On the multivariate runs test. *The Annals of Statistics* 27(1), 290–298.
- Holmes, S. and W. Huber (2018). *Modern statistics for modern biology*. Cambridge University Press.
- Huang, M., J. Wang, E. Torre, H. Dueck, S. Shaffer, R. Bonasio, J. I. Murray, A. Raj, M. Li, and N. R. Zhang (2018). Saver: gene expression recovery for single-cell rna sequencing. *Nature methods* 15(7), 539.
- Hwang, B., J. H. Lee, and D. Bang (2018). Single-cell rna sequencing technologies and bioinformatics pipelines. *Experimental & molecular medicine* 50(8), 1–14.
- Jaitin, D. A., E. Kenigsberg, H. Keren-Shaul, N. Elefant, F. Paul, I. Zaretsky, A. Mildner, N. Cohen, S. Jung, A. Tanay, et al. (2014). Massively parallel single-cell rna-seq for marker-free decomposition of tissues into cell types. *Science* 343(6172), 776–779.
- Janson, S. (1984). Bounds on the distributions of extremal values of a scanning process. *Stochastic processes and their applications* 18(2), 313–328.
- Jia, C., Y. Hu, D. Kelly, J. Kim, M. Li, and N. R. Zhang (2017). Accounting for technical noise in differential expression analysis of single-cell rna sequencing data. *Nucleic acids research* 45(19), 10978–10988.
- Jiang, H., L. L. Sohn, H. Huang, and L. Chen (2018). Single cell clustering based on cell-pair differentiability correlation and variance analysis. *Bioinformatics* 34(21), 3684–3694.
- Kozachenko, L. F. and N. N. Leonenko (1987). Sample estimate of the entropy of a random vector. *Problemy Peredachi Informatsii* 23(2), 9–16.
- Last, G. and M. Penrose (2017). *Lectures on the Poisson process*, Volume 7. Cambridge University Press.

- Linderman, M. D., Z. Bjornson, E. F. Simonds, P. Qiu, R. V. Bruggner, K. Sheode, T. H. Meng, S. K. Plevritis, and G. P. Nolan (2012, September). Cytospade: high-performance analysis and visualization of high-dimensional cytometry data. *Bioinformatics* 28(18), 2400–2401.
- Maaten, L. v. d. and G. Hinton (2008). Visualizing data using t-sne. *Journal of machine learning research* 9(Nov), 2579–2605.
- Mack, Y. P. (1983). Rate of strong uniform convergence of k -nn density estimates. *Journal of statistical planning and inference* 8(2), 185–192.
- Mack, Y. P. and M. Rosenblatt (1979). Multivariate k -nearest neighbor density estimates. *Journal of Multivariate Analysis* 9(1), 1–15.
- Matheson, N. J., J. Sumner, K. Wals, R. Rapiteanu, M. P. Weekes, R. Vigan, J. Weinelt, M. Schindler, R. Antrobus, A. S. Costa, et al. (2015). Cell surface proteomic map of hiv infection reveals antagonism of amino acid metabolism by vpu and nef. *Cell host & microbe* 18(4), 409–423.
- Michel, N., I. Allespach, S. Venzke, O. T. Fackler, and O. T. Keppler (2005). The nef protein of human immunodeficiency virus establishes superinfection immunity by a dual strategy to downregulate cell-surface ccr5 and cd4. *Current Biology* 15(8), 714–723.
- Niculescu, C. P. and F. Popovici (2011). A note on the behavior of integrable functions at infinity. *Journal of Mathematical Analysis and Applications* 381(2), 742–747.
- Penrose, M. D. and J. E. Yukich (2003). Weak laws of large numbers in geometric probability. *The Annals of Applied Probability* 13(1), 277–303.
- Qiu, P. (2012, 05). Inferring phenotypic properties from single-cell characteristics. *PLoS ONE* 7(5), e37038.
- Rosenbaum, P. R. (2005). An exact distribution-free test comparing two multivariate distributions based on adjacency. *Journal of the Royal Statistical Society: Series B (Statistical Methodology)* 67(4), 515–530.
- Ross, T. M., A. E. Oran, and B. R. Cullen (1999). Inhibition of hiv-1 progeny virion release by cell-surface cd4 is relieved by expression of the viral nef protein. *Current biology* 9(12), 613–621.
- Samworth, R. J. (2012). Optimal weighted nearest neighbour classifiers. *The Annals of Statistics* 40(5), 2733–2763.

- Schiffman, C., C. Lin, F. Shi, L. Chen, L. Sohn, and H. Huang (2017). Sideseq: a cell similarity measure defined by shared identified differentially expressed genes for single-cell rna sequencing data. *Statistics in biosciences* 9(1), 200–216.
- Schilling, M. F. (1986). Multivariate two-sample tests based on nearest neighbors. *Journal of the American Statistical Association* 81(395), 799–806.
- Sen, A., M. E. Rothenberg, G. Mukherjee, N. Feng, T. Kalisky, N. Nair, I. M. Johnstone, M. F. Clarke, and H. B. Greenberg (2012). Innate immune response to homologous rotavirus infection in the small intestinal villous epithelium at single-cell resolution. *Proceedings of the National Academy of Sciences* 109(50), 20667–20672.
- Sen, N., G. Mukherjee, and A. M. Arvin (2015). Single cell mass cytometry reveals remodeling of human t cell phenotypes by varicella zoster virus. *Methods* 90, 85–94.
- Sen, N., G. Mukherjee, A. Sen, S. C. Bendall, P. Sung, G. P. Nolan, and A. M. Arvin (2014). Single-cell mass cytometry analysis of human tonsil t cell remodeling by varicella zoster virus. *Cell reports* 8(2), 633–645.
- Shi, F. and H. Huang (2017). Identifying cell subpopulations and their genetic drivers from single-cell rna-seq data using a biclustering approach. *Journal of Computational Biology* 24(7), 663–674.
- Swigut, T., N. Shohdy, and J. Skowronski (2001). Mechanism for down-regulation of cd28 by nef. *The EMBO journal* 20(7), 1593–1604.
- Tibshirani, R. and G. Walther (2005). Cluster validation by prediction strength. *Journal of Computational and Graphical Statistics* 14(3), 511–528.
- Vasicek, O. (1976). A test for normality based on sample entropy. *Journal of the Royal Statistical Society: Series B (Methodological)* 38(1), 54–59.
- Vassena, L., E. Giuliani, H. Koppensteiner, S. Bolduan, M. Schindler, and M. Doria (2015). Hiv-1 nef and vpu interfere with l-selectin (cd62l) cell surface expression to inhibit adhesion and signaling in infected cd4+ t lymphocytes. *Journal of virology*, JVI-00611.
- Wang, J., M. Huang, E. Torre, H. Dueck, S. Shaffer, J. Murray, A. Raj, M. Li, and N. R. Zhang (2018). Gene expression distribution deconvolution in single-cell rna sequencing. *Proceedings of the National Academy of Sciences* 115(28), E6437–E6446.

- Weiss, L. (1960). Two-sample tests for multivariate distributions. *The Annals of Mathematical Statistics*, 159–164.
- Xue-Kun Song, P. (2000). Multivariate dispersion models generated from gaussian copula. *Scandinavian Journal of Statistics* 27(2), 305–320.
- Yukich, J. (2013). Limit theorems in discrete stochastic geometry. In *Stochastic geometry, spatial statistics and random fields*, pp. 239–275. Springer.
- Yukich, J. E. (2006). *Probability theory of classical Euclidean optimization problems*. Springer.
- Zhang, J. and H. Chen (2017). Graph-based two-sample tests for discrete data. *arXiv preprint arXiv:1711.04349*, 2017.